Dislocation networks in precipitation hardened aluminium alloys during plastic deformation

The effects of dislocations on the anelastic behaviour and the evolution of dislocation networks in an AA7075 aluminium alloy.

Guido Smits

Thesis

submitted in partial fulfilment of the requirements for the degree of

Master of Science

in the department of

Materials Science and Engineering

at the

Faculty of Mechanical, Maritime and Materials Engineering

of

Delft University of Technology

Department of Materials Science and Engineering
Faculty of Mechanical, Maritime and Materials Engineering
Delft University of Technology
Delft, The Netherlands

Author:	Guido Smits
Student Number:	4512219
Date:	June 15, 2018

Thesis Committee:

Chair:	Prof. Dr. Ir J. Sietsma	Faculty 3mE, TU Delft
Committee Member:	Dr. A.J. Böttger	Faculty 3mE, TU Delft
Committee Member:	Dr. N. Irani	Faculty 3mE, TU Delft
Committee Member:	Dr. P. van Liempt	Faculty 3mE, TU Delft

Abstract

The effects of precipitates in the microstructure of an AA7075 aluminium alloy on: the dislocation behaviour, dislocation structure and dislocation structure evolution during plastic deformation were investigated using the physical yield criterion model by van Liempt and Sietsma [1]. The model was in fact applied for the first time to aluminium and an AA7075 aluminium alloy. By constructing an extended Kocks-Mecking plot from the measured tensile and interrupted tensile data the dislocation density, average dislocation segment length and physical yield stress were determined.

The aim of the present study was to get a better understanding of the role of precipitates in the evolution of the dislocation structure during plastic deformation. The recovery of anelastic strain during loading and subsequent unloading after plastic deformation was investigated as well. The yield criterion was used to study the anelastic loading, while a constitutive unloading model by Torkabadi et al. [2] was used to study the unloading behaviour. The models were combined to define the fraction of unrecoverable anelastic strain. The anelastic strain is related to springback. Therefore a better understanding of the anelastic strain could be useful for making better predictions of springback after metal forming. The physical yield criterion was further extended by incorporating a continuous uniform dislocation segment length distribution. Insight on the dislocation segment length distribution, and the evolution thereof during plastic deformation, could help to better understand the mechanical behaviour of metals.

The evolution of the dislocation structure during plastic deformation is impeded by the presence of precipitates in the microstructure. Therefore, the physical interpretation of α in the Taylor equation which quantifies the dislocation structure, proposed by Arachebelata et al. [3], was modified to incorporate the effects of precipitates in the microstructure. The dislocation structure parameter α should remain constant. However, the average dislocation segment length obtained from the extended Kocks-Mecking plot does not decrease sufficiently to accommodate a constant α. The introduction of the length between precipitates, which is independent from work hardening, into the Taylor equation ensures that α does remain constant, whilst in addition it provides an estimate of the distance between the precipitates.

Anelastic strain, caused by reversible glide of dislocations in the pre-yield regime, is introduced into or recovered from the metal during loading and unloading respectively. The anelastic unloading strain determined from the interrupted tensile tests was found to be smaller than what was expected according to the model. Three possible causes were identified: not all Frank-Read sources are at their critical state when unloading is initiated, dislocation loops propagating through the crystal undo portions of the anelastic unloading strain and the retracting dislocations remain stuck behind obstacles whilst retracting under the reducing applied stress. The constitutive model was found to be not suitable for studying the dislocation behaviour during unloading because the change of dislocation segment length with plastic deformation is not accounted for. The development of a physical unloading model is therefore recommended.

The distribution of the dislocation segment lengths could explain the non-zero value of the work hardening rate Θ at the abrupt change of slope between the pre and post-yield regime in the extended Kocks-Mecking plot. The value of Θ at this point could be an indication of the distribution width. The continuous uniform distribution is a rather unrealistic description of the dislocation segment length distribution. Therefore, other distribution types are proposed for the further development of the dislocation segment length distribution model of the physical yield criterion.

Acknowledgements

With this thesis comes an end to my time as student at the Delft University of Technology where I spent the last two years fulfilling all the requirements for my degree in Materials Science and Engineering. After a period of eight months my Master's thesis is finally completed and only one thing remains and that is to give credit, where credit is due. First of all, I would like to thank Prof. Dr. Ir. Jilt Sietsma for giving me the freedom to define my own research and helping me find the right direction while doing so. Also, for helping and supervising me for the duration of my Master's thesis. For the endless discussions on dislocations, the physical yield criterion and everything else metallurgically, I want to express great appreciation to Dr. Peter van Liempt. I would also like to thank Em. Prof. Dr. Ir. Jan van Turnhout for the many fruitful discussions about my thesis and explaining how to introduce distributions into the physical yield criterion model. For the experimental work done in context of this thesis at the Department of Materials Science and Engineering of the Delft University of Technology I would like to thank everybody involved with the preparation of the specimens or the actual testing. For the mechanical testing I would like to thank Dr. Ir. Ton Riemslag and Elise Reinton for the discussions on tensile testing and help in setting up the experiments. The heat treatments of my specimens would not have been possible without the help of Hans Hofman and without Wim Velt and Reinier van Antwerpen, there would not have been appropriate specimens in the first place. Also, I would like to thank Sander van Asperen for his help with polishing the samples before X-ray analysis and Ruud Hendrikx for performing the X-ray analysis. Finally, I would like to thank everyone else who had to bear with me for the past eight months.

Guido Smits
Delft
June 15, 2018

Contents

List of Symbols **6**

1 Introduction **8**

2 Theoretical Background **10**

2.1 Pinning of dislocations 10

2.1.1 Lomer locks 11

2.1.2 Lomer-Cottrell locks 11

2.1.3 Hirth locks 12

2.1.4 Pinning by other agents than dislocations 13

2.2 Frank-Read sources 13

2.2.1 Frank-Read sources and dislocation networks 15

2.3 The Orowan mechanism 15

2.4 Dislocation behaviour in the pre-yield regime 17

2.4.1 Applications of the physical yield criterion 19

2.4.2 Limitations of the physical yield criterion 20

2.4.3 The Orowan mechanism and the physical yield criterion 20

2.5 Anelastic dislocation behaviour under cyclic plastic loading 21

2.5.1 Unloading and reloading behaviour 21

2.5.2 Anelastic behaviour during unloading 22

2.5.3 Recovery of anelastic strain 23

2.5.4 Anelastic strain models and the dislocation segment length and density . 24

2.6 Dislocation segment length distribution 25

2.6.1 Distributed dislocation length and the physical yield criterion 25

2.6.2 Influence of the length distribution on the anelastic pre-yield behaviour . 28

2.7 Summary 28

3 Experimental Details **30**

3.1 Materials 30

3.1.1 Chemical compositions 30

3.1.2 Heat treatments 31

3.2 Method 31

3.2.1 Equipment 32

4 Results **34**
4.1 Tensile tests results . . . 34
4.1.1 Tensile testing results - Pure Al . . . 34
4.1.2 Tensile testing results - AA7075 . . . 35
4.1.3 Dislocation segment length distribution - AA7075 . . . 38
4.2 Interrupted tensile tests . . . 40
4.2.1 Results of the interrupted tensile tests . . . 40
4.2.2 Fitting the Taylor equation . . . 41
4.2.3 Anelastic strain during unloading . . . 42

5 Discussion **46**
5.1 The physical yield criterion for aluminium and AA7075 . . . 46
5.1.1 Anomalies in tensile testing results . . . 46
5.2 Interrupted tensile testing experiments . . . 46
5.3 Effects of Precipitation hardening . . . 47
5.3.1 Precipitates and the evolution of dislocation segment length . . . 48
5.4 Anelastic Strain Recovery . . . 51
5.4.1 Constitutive model of Torkabadi et al. . . . 52
5.5 Distribution of dislocation segment length . . . 53
5.5.1 Alternative distribution types . . . 53
5.5.2 Number density length distribution . . . 54

6 Conclusions and Recommendations **56**
6.1 Conclusions . . . 56
6.2 Recommendations . . . 57

References **58**

List of Symbols

α	Dislocation structure parameter
α_f	Dislocation type constant in Frank's rule
a	Lattice parameter
A	Area swept by dislocation
A_S^{UL}	Average swept area by a Frank-Read source during unloading
β	Dislocation network geometrical constant in the distribution of Shi and Northwood
b	Magnitude of the Burgers vector
ε	Tensile strain
ε_{el}	Elastic tensile strain
ε_{ae}	Anelastic tensile strain
ε_p	Remaining tensile strain after unloading
ε_{pl}	Plastic tensile strain
ε_{pre}	Pre-yield tensile strain
ε_t	Total tensile strain upon loading
E	Young's Modulus
E_{el}	Energy of a dislocation
ϕ	Angle of the area swept by a Frank-Read source
Φ	Dislocation segment length distribution of Shi and Northwood
f_p	Volume fraction of particles
f_{UR}	Fraction of unrecoverable anelastic strain
γ	Shear strain
G	Shear Modulus
h	Box width of the dislocation density length distribution
I_ρ	Integral of S for the dislocation density distributed box model
I_N	Integral of S for the dislocation number density distributed box model
K	Fitting parameter in the constitutive unloading model of Torkabadi et al.
L	Distance between dislocation pinning points
L_0	Length of the longest dislocation
L_d	Distance between nodes if only dislocation-dislocation interaction is considered
L_p	Distance between precipitates
L_m	Dislocation segment length at the maximum of Φ
L_A	Average dislocation length in a dislocation segment length distribution
$\overline{M}$	Taylor factor
N	Dislocation number density
ν	Poisson's ratio

ρ	Dislocation density
ρ_0	Dislocation density in distributed model
ρ_i	Initial dislocation density
r	Radius of dislocation segment
r_p	Particle radius
σ	Tensile stress
σ_0	Yield stress contribution in absence of dislocations
σ_c	Physical yield stress
σ_{c0}	Physical yield stress associated with the length ratio u_0
σ_d	The stress contribution due to dislocation self-interaction
σ_f	Flow stress
$\sigma_{R_{p0.2}}$	0.2% strain offset yield stress
σ_y	Physical yield stress in the model of Torkabadi et al.
s	Normalized stress parameter
S	Stress dependent part of the pre-yield anelastic modulus
τ	Resolved shear stress
τ_c	Critical resolved shear stress
τ_{or}	Orowan shear stress
Θ	Work hardening rate
Θ_{AE}	Work hardening rate due to anelastic strain
Θ_{PRE}	Pre-yield anelastic modulus
Θ_{AE}^{γ}	Work hardening rate due to anelastic shear strain
Θ_c	Work hardening rate at the physical yield stress
T_{ND}	Non-distributed normalized work hardening rate
T_D	Distributed normalized work hardening rate
u	Length ratio in the distributed pre-yield anelastic modulus
u_0	Length ratio in the distributed model normalized to average length
V	Stress independent part of the pre-yield anelastic modulus
w	Box width in the number density length distribution
X	Geometrical factor dependent on the type of dislocation

CHAPTER 1

Introduction

In mechanical engineering practice the yield stress of a metal is almost always determined using the 0.2% strain offset. In this method the intersection of the stress-strain curve with a line parallel to the elastic one and shifted by 0.2% strain is used to determine the yield stress of the metal. The value of 0.2% is however arbitrarily chosen and has no physical foundation. Van Liempt and Sietsma [1] propose that the physical yield stress of a metal is the stress at which regenerative multiplication of dislocations occurs. In their physical yield criterion model, they consider Frank-Read sources as the regenerative dislocation multiplication mechanism. An extended Kocks-Mecking plot can be used to graphically determine the physical yield stress which presents itself as an abrupt change of slope, indicating the transition of the pre-yield to the post-yield regime. An extended Kocks-Mecking plot shows the work hardening rate ($\Theta = \mathrm{d}\sigma/\mathrm{d}\varepsilon$) as a function of the applied stress (σ). The curvature of the extended Kocks-Mecking plot in the pre-yield regime also shows that the elastic behaviour in the pre-yield regime is not strictly linear. This non-linear elastic behaviour is referred to as anelasticity [4]. According to Zener, anelasticity is due to relaxation effects. However, anelasticity can also be attributed to the reversible glide of dislocations in the pre-yield regime [1, 5]. Reversible glide means that dislocations already move through the lattice at stresses below the yield stress and that the strain induced hereby can be superimposed on the strains caused by the linear elastic Hooke's law. The glide of these dislocations is reversible, meaning that they can return upon unloading, recovering the anelastic strain. Anelasticity has also been related to springback, a phenomenon whereby a metal changes its shape due to (an)elasticity during unloading after plastic deformation [6, 7]. Springback has also been linked to anelasticity in the sense of reversible dislocation movement, where the retraction of the dislocation segments in Frank-Read sources are the origin of anelastic strain during unloading [3, 8]. Better understanding of the anelastic strain behaviour during unloading could improve the analysis and modelling of springback, resulting in an increased accuracy in industrial forming processes.

Dislocations in metal form a network where intersections of different dislocation lines form nodes. Some nodes form locks which pin dislocations. In the physical yield criterion an average dislocation segment length between dislocation pinning points is used. The average dislocation segment length decreases when the material work hardens during plastic deformation. Dislocations also interact with other microstructural features such as solute atoms, vacancies, grain boundaries and precipitates. In a precipitated metal the precipitates form a relatively static part of the dislocation pinning structure, meaning their spacing does not change as the material work hardens. Dislocations bow out between the precipitates like Frank-Read sources, and such behaviour can readily be introduced in the physical yield criterion. The aim of the present study is to better understand the effects of a partially static dislocation pinning structure due to a precipitated microstructure on the dislocation behaviour and evolution of the dislocation structure in metals during plastic deformation. The dislocation structure in a metal governs its mechanical behaviour. Therefore the study of dislocation behaviour in the dislocation network as well as the evolution of the dislocation network is of particular interest to better understand and predict the mechanical behaviour of metals.

Conventional tensile and interrupted tensile testing according to [3] were applied in combination with the theory of the yield criterion of van Liempt and Sietsma [1] and the constitutive model of Torkabadi et al. [2]. It was found that a precipitated microstructure in the aluminium alloy impeded the decrease of the average segment length during work hardening. A new expression for the dislocation structure parameter α in the Taylor equation is proposed which includes: the average length separating the precipitates, the average dislocation segment length and dislocation density. The modified expression for α was validated according to the same method used by Arechabaleta et al. [3]. Another important aspect is the unloading behaviour after plastic deformation. The anelastic behaviour of dislocation sources retracting to their equilibrium position is considered as one of the causes of springback. An attempt was made to study the recovery of anelastic strain during unloading using the constitutive model of Torkabadi et al. [2]. The model was found to be unsuitable on a physical basis to study the dislocation behaviour during unloading of metals. So, the development of a physically based unloading model is required for further study on the anelastic behaviour during unloading and the recovery of anelastic strain. The yield criterion uses an average dislocation segment length. The dislocation structure in a metal is however never completely homogeneous and therefore a distribution of the dislocation segment lengths has to be considered. Quantification of the dislocation segment length distribution could help to further the understanding of mechanical behaviour of metals. This work presents a basic continuous uniform length distribution as a first introduction of dislocation segment length distributions into the physical yield criterion. The length distribution introduces an extra fitting parameter, representing the width of the distribution. It was found that a length distribution could explain why the Kocks-Mecking plot does not drop to zero at the onset of plastic deformation. The development of length distributions using realistic distributions for the dislocation segment length is advised. This could be used to study the evolution of the dislocation structure during work hardening in greater detail.

In chapter 2 the theoretical background of this work is presented. First key concepts related to dislocation pinning, dislocation multiplication (Frank-Read sources) and impediment of dislocation movement (Orowan mechanism) are discussed. Knowledge of these mechanisms is required to understand the mechanisms behind anelastic behaviour during the loading and unloading of metals. Two models, one for loading and one for unloading of metals during tensile tests are discussed next. For loading the physical yield criterion by van Liempt and Sietsma [1] and for unloading a constitutive model by Torkabadi et al. [2], which uses similar concepts as the physical yield criterion. These models are combined to quantify the anelastic strain during loading and unloading and to investigate the recovery of anelastic strain. Finally, the yield criterion is extended by introducing a continuous uniform distribution of the length of dislocation segments. Chapter 3 covers the alloys used in the current study as well as the testing methods. A novelty of the present study is the application of the physical yield criterion to a metal other than steel, namely aluminium and an aluminium alloy. An Al-Mg-Zn based commercial 7075 alloy was used, which was age-hardened for 0, 16, 24 and 32 hours before the specimens were machined. The specimens were subjected to conventional tensile tests as well as interrupted tensile tests with incremental plastic strain. The results of the tensile and interrupted tensile tests are presented in chapter 4 and discussed in chapter 5. Finally, conclusions of this study and recommendations for future work are presented in chapter 6.

CHAPTER 2

Theoretical Background

The effects of dislocations and dislocation structures on the anelastic behaviour of aluminium and aluminium alloys were investigated. The effect of a precipitated microstructure, providing additional pinning of dislocations in the metal, was considered as well. To understand the effects it is important to understand the mechanisms underlying the multiplication of dislocations. One of the main multiplication mechanisms, the Frank-Read source is considered in the model of van Liempt and Sietsma [1]. The pinning of dislocations required for the operation of Frank-Read source is investigated first. Subsequently, the Frank-Read mechanism itself was studied as well. The Orowan mechanism describes the behaviour of dislocations in a precipitated matrix. The behaviour of dislocations shares some of its features, namely the bowing out of dislocation line segments, with the Frank-Read source. The model by van Liempt and Sietsma considers the movement of dislocations as the origin of reversible anelasticity, the non-linear elastic behaviour of a metal [1]. This anelasticity is also related to springback [3,6,7], a technological phenomenon in which a metal part changes its geometrical shape after forming, upon unloading it does not maintain the shape imposed by the die. Springback therfore affects the dimensional accuracy of the component. Anelastic behaviour is often studied by loading and unloading a metal in a tensile test, this is also referred to as an interrupted tensile test [2, 3, 8, 9]. For analysing the loading and unloading two models are considered: in section 2.4 the physical yield criterion for loading by van Liempt and Sietsma [1] and in section 2.5 a constitutive model by Torkabadi et al. during unloading [2]. Both models use the dislocation density and average dislocation segment length (of the Frank-Read source) as fitting parameters. The evolution of these parameters with strain shows however that care has to be taken when comparing the values of these parameters. Both the loading and unloading model quantify the reversible anelastic behaviour of a metal. A method is proposed to calculate the recovery of anelastic deformation due to the reversible movement of dislocations. Lastly, an addition is made to the model of van Liempt and Sietsma by introducing a distribution for the dislocation segment length. This is done using a continuous uniform distribution which gives an analytical solution.

2.1 Pinning of dislocations

For the understanding of the mechanisms involved in the motion and impediment of dislocations, it is important to realize the origin of the pinning of dislocation lines. This section briefly discusses three mechanisms of dislocation self-interaction, which result in pinning points for the two interacting dislocations which become locked as a result. Such a lock is also called a sessile dislocation which is not able to glide unless at the stress becomes very high, in contrast to glissile dislocations [10]. The mechanisms discussed are the Lomer lock [11], Lomer-Cottrell lock [12] and the Hirth lock [13] mechanisms. In addition one mechanism describing the interaction between dislocations and particles in the matrix, the Orowan mechanism [14], is explained in section 2.3. Other pinning mechanisms based on the interaction of a dislocation with other microstructural pinning features are briefly mentioned.

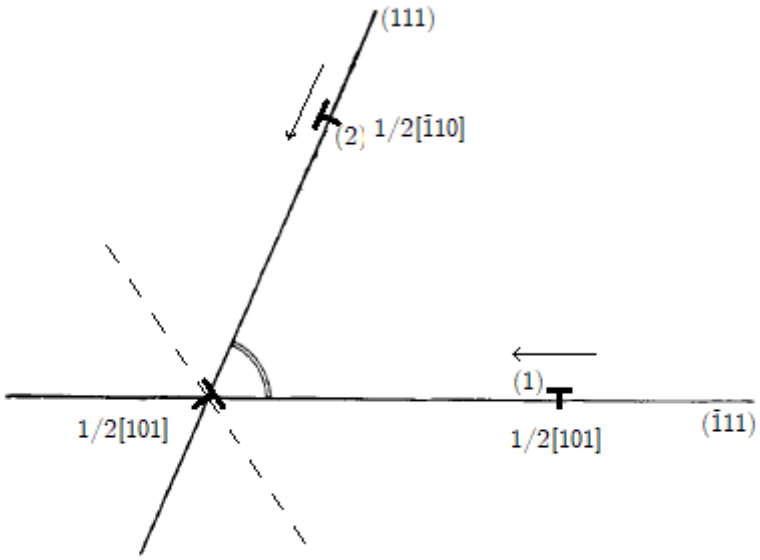

Figure 2.1: Schematic representation of a Lomer lock, showing two dislocations on the $(\bar{1}11)$ and (111) plane gliding towards an intersection where they recombine into a dislocation of the form $\frac{1}{2}[101]$. Figure adapted from: [11, 15].

2.1.1 Lomer locks

The Lomer lock considers two dislocations on two slip planes. Usually, two of the easy slip planes of the face centered cubic crystal structure are considered. When the dislocations meet at the intersection of the two planes (figure 2.1) they recombine to become a single immobile or sessile dislocation. Initially, the mechanism was proposed by Lomer who considered the combined dislocation as sessile [11], however Cottrell [12] pointed out that it is not sessile in the sense used by Frank [10].

Suppose that the two slip planes are the $(\bar{1}11)$ and (111) planes which intersect along $[0\bar{1}1]$. Dislocations moving along these planes have the Burgers vectors $\frac{1}{2}[\bar{1}10]$ and $\frac{1}{2}[101]$ respectively. When the two dislocations come together they react according to:

$$\frac{1}{2}[\bar{1}10] + \frac{1}{2}[101] \rightarrow \frac{1}{2}[011] \tag{2.1}$$

The new dislocation now has a Burgers vector $\frac{1}{2}[011]$ and has only half the energy per unit length according to Frank's rule [16]. The glide plane of the combined dislocation is (100), which is not a slip plane in the FCC crystal structure. This means that the combined dislocation is unable to glide. This mechanism can also be visualized using Thompson's tetrahedron (figure 2.2) [17]. The two dislocations indicated by **DA** and **BD**, react to form **BA**, a dislocation unable to glide.

2.1.2 Lomer-Cottrell locks

Cottrell [12] extended the lock mechanism proposed by Lomer by introducing partial dislocations. Partial dislocations form, because the elastic strain energy is lowered according to Frank's rule, which states that the elastic energy of a dislocation equals $E_{el} = \alpha_f G b^2$, where $\alpha_f \approx 0.5 - 1.0$ is a constant representing the type of dislocation and and G the shear modulus. The energy is thus proportional to b^2 [15, 16]. Hence the formation of two partial dislocations is more favourable than a perfect dislocation because the magnitude of b is then smaller. This is illustrated in figure 2.2. In the Lomer-Cottrell lock the two dislocations on the slip planes disassociate into two partial dislocations. The leading partial dislocations meet at the intersection of the planes and either attract or repel each other. Each slip plane has three possible

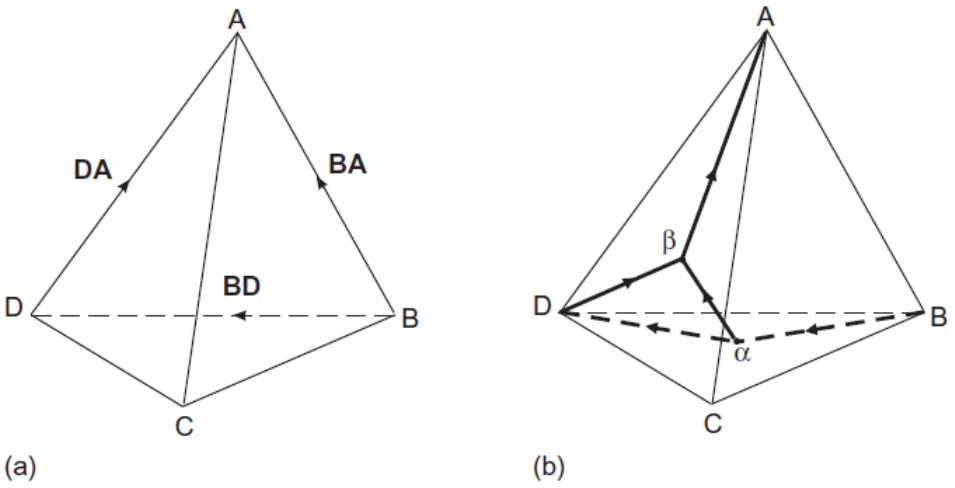

Figure 2.2: The Lomer lock (a) and the Lomer-Cottrel lock (b) illustrated using Thompson's tetrahedron. The edges represent the slip planes in the FCC lattice, and the vector sums of the edges give the resulting dislocation. Partial dislocations are indicated by the α and β. Figure from: [15].

$\frac{1}{6}\langle 112\rangle$ vectors, including their reverses. In total 36 combinations have to be considered [15]. The reaction resulting in the largest reduction in energy according to Frank's rule is of the form $\frac{1}{6}\langle 110\rangle$ [16]. An example is shown considering the same planes as in the Lomer lock [15] in figure 2.3.

The dislocations gliding on the $(\bar{1}11)$ and (111) planes disassociate into two partial dislocations each (figure 2.3). On the $(\bar{1}11)$ plane,

$$\frac{1}{2}[\bar{1}10] \rightarrow \frac{1}{6}[\bar{1}2\bar{1}] + \frac{1}{6}[\bar{2}11] \tag{2.2}$$

and on the (111) plane,

$$\frac{1}{2}[101] \rightarrow \frac{1}{6}[1\bar{1}2] + \frac{1}{6}[211]. \tag{2.3}$$

The first partial dislocations from both planes meet at the intersection, just like in the Lomer lock mechanism. These partial dislocation react to form a new dislocation with Burgers vector:

$$\frac{1}{6}[\bar{1}2\bar{1}] + \frac{1}{6}[1\bar{1}2] \rightarrow \frac{1}{6}[011], \tag{2.4}$$

which according to Frank's rule [16] is of lower energy per unit length. The Burgers vector of the resulting dislocation does not lie in the slip plane and thus it is not able to glide. The Lomer-Cottrell lock can also be visualized in Thompson's tetrahedron. The dislocation **DA** disassociates into $\mathbf{D}\boldsymbol{\beta}$ and $\boldsymbol{\beta}\mathbf{A}$. The second dislocation (**BD**) disassociates into $\mathbf{B}\boldsymbol{\alpha}$ and $\boldsymbol{\alpha}\mathbf{D}$. Two of the partial dislocations then recombine to form:

$$\boldsymbol{\alpha}\mathbf{D} + \mathbf{D}\boldsymbol{\beta} = \boldsymbol{\alpha}\boldsymbol{\beta} \tag{2.5}$$

where $\boldsymbol{\alpha}\boldsymbol{\beta}$ represents the immobile vector of the form $\frac{1}{6}\langle 110\rangle$. A graphical representation is shown in figure 2.2.

2.1.3 Hirth locks

Hirth [13] described the interactions between dislocations in the FCC lattice based on Thompson's tetrahedron. One of these interactions became known as the Hirth lock. It involves two dislocations, **BD** and **AC**. These two dislocations react to form a new $< 100 >$ type dislocation which is immobile [15].

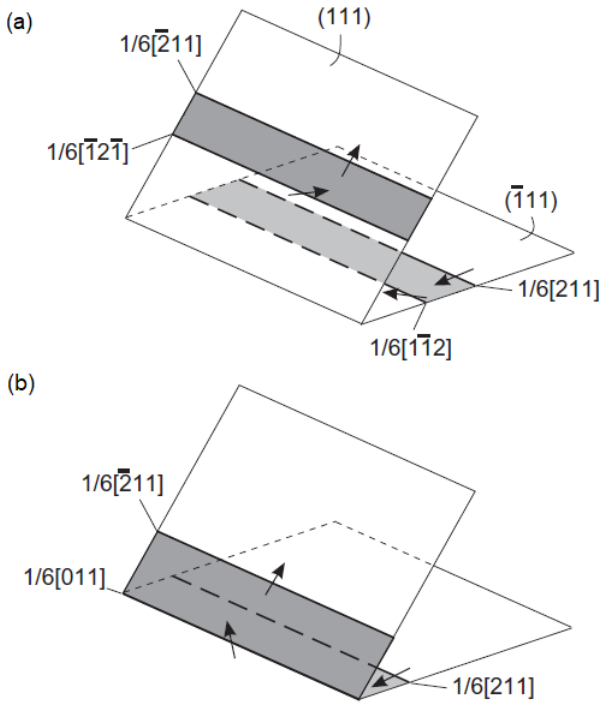

Figure 2.3: Two sets of partial dislocation gliding on the ($\bar{1}$11) and (111) plane (a). The two leading partial dislocations react to form a Lomer-Cottrell lock (b), Figure adapted from: [15]

2.1.4 Pinning by other agents than dislocations

Interaction with other dislocations is not the only mechanism through which a dislocation can become locked or immobile. Impurities in the lattice can also pin dislocations in their stress fields, but solute atoms and vacancies as well. The introduction of precipitates or dispersoids also results in extra boundaries and pinning points for the dislocations. Grain boundaries also affect the mobility of dislocations [18, 19]. The effects of the grain size are quantified through the Hall-Petch relation. However the effects of grain size in the pre-yield regime has not been extensively studied. Van Liempt et al. [20] extended their yield criterion to incorporate the Hall-Petch effect. Their model is based on the strain incompatibility of grains upon elastic deformation due to the orientation differences with respect to the tensile axis. The grain size effects are not considered in the current research and therefore not further investigated. It should however be noted that the contribution of the grain size can become significant, if the grain size of the metal is reduced.

2.2 Frank-Read sources

To accomodate the plastic strain introduced during plastic deformation in metals, the regenerative multiplication of dislocations is required. One of the possible mechanisms for regenerative multiplication is the Frank-Read source [1]. A Frank-Read source consists of a segment of dislocation line of which the Burgers vector lies in the slip plane. Each end is pinned, which can be caused by: dislocation intersections, dislocation nodes, composite jogs, precipitates or other barriers [3, 15, 18, 19, 21]. When a resolved shear stress is applied the dislocation line segment bows out (figure 2.4 (b)) reducing the radius of curvature [22]. The line stress of a dislocation with Burgers vector b and a radius r is approximately:

$$\tau = \frac{Gb}{2r}. \tag{2.6}$$

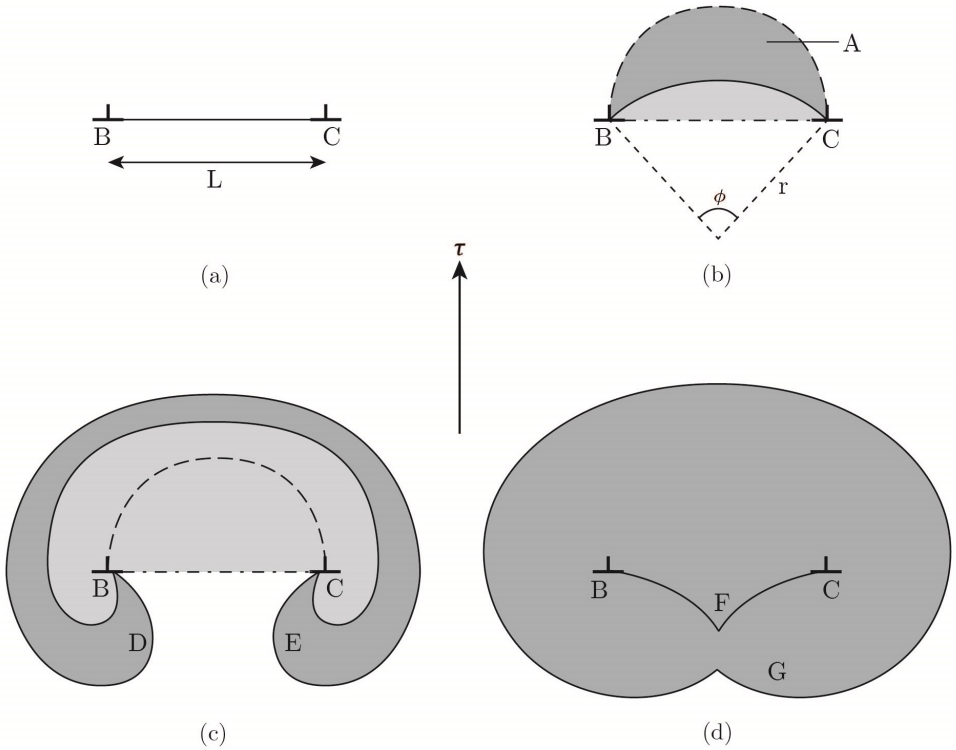

Figure 2.4: A Frank-Read source made up of a dislocation line segment between B and C (a). The resolved shear stress τ causes the dislocation line to bow out (b) and spiral around B and C (c) until a loop forms at D and E (d), the process then repeats itself. The scale of L is in the order of 100 nm. Figure adapted from: [1, 15, 22]

When a dislocation segment bows out such that $L = 2r$ the Frank-Read source reaches its critical state. The value r reaches a minimum value and if the resolved shear stress is increased above this critical stress the dislocation becomes unstable and can no longer satisfy equation (2.6) [15]. The critical resolved shear stress of a Frank-Read source is then given by:

$$\tau_c = \frac{Gb}{L}. \tag{2.7}$$

Ashby proposed a more accurate description for the critical stress:

$$\tau_c = X\frac{Gb}{2\pi L}\ln\left(\frac{L}{b}\right) \tag{2.8}$$

where $X = 1$ for an edge dislocation and $X = (1-\nu)^{-1}$ for a screw dislocation [23]. This expression is however seldom used, instead equation (2.6) is preferred. When the resolved shear stress is increased further after the critical state is reached, the dislocation line starts spiralling around the pinning points B and C (figure 2.4 (c)), reducing the curvature of the line segment. It continues to reduce its curvature by spiralling around the pinning points until the dislocation lines at points D and E meet. The line segments at D and E are of opposing signs meaning that when they meet they annihilate causing the formation of a loop as well as a new segment between A and B (figure 2.4 (d)). The loop starts propagating through the lattice whereas the new segment starts the process over again.

The area (highlighted in grey in figure 2.4) which is covered by the bowing out of the dislocation segment, is related to the strain accommodated by the movement of dislocations and is given by:

$$A = \frac{1}{2}r^2(\phi - \sin\phi) \tag{2.9}$$

where $r > \frac{L}{2}$ and with the value for the angle ϕ [24]

$$\phi = 2 \arcsin\left(\frac{L}{2r}\right). \tag{2.10}$$

2.2.1 Frank-Read sources and dislocation networks

The Frank-Read source is based on a single dislocation segment. In reality a network of dislocations is present in the material, the Frank network (figure 2.5) [15, 21, 25]. In the Frank network dislocation segments are connected at nodes and form a three dimensional dislocation structure. Dislocations in the Frank network form cells of roughly equal size. Observations of such network have shown that they exist with a size in the order of microns [21].

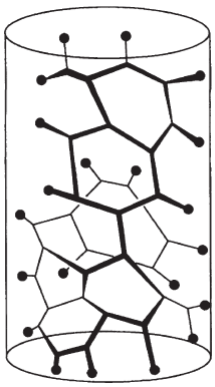

Figure 2.5: A schematic representation of a Frank Network. Figure from: [15, 25]

A single Frank-Read source on an infinite plane activated by a resolved shear stress larger than the critical resolved shear stress can emit dislocation loops as long as the supercritical stress is maintained. The loops can then travel indefinitely. In reality the travel of the dislocation loop is impeded, in the first place by the size of the grain but also by other dislocations intersecting the glide plane. Such dislocations, called forest dislocations form obstacles for the propagating loop. The propagating loop can cut through the forest dislocations and in some cases form a jog in the process. These jogs contribute little to the work hardening of the metal. The forest dislocations also affect the shape of the emitted Frank-Read loop. The loop is no longer of circular shape but instead curves in between the forest dislocation [15, 21].

The emission of dislocation loops by Frank-Read sources in the metal increases the possibility that dislocations meet according to the locking situation described in 2.1, causing new locks to form in the already existing dislocation structure. As such the length of the segments in the Frank network decrease when the dislocation density ρ is increased by regenerative multiplication of dislocations.

2.3 The Orowan mechanism

The mechanism describing the interaction between precipitates and dislocations proposed by Orowan considers a gliding dislocation which encounters particles, for instance precipitates or dispersoids. In this case precipitates will be considered. The dislocation line will bow out between the precipitates (figure 2.6). This occurs much alike the Frank-Read mechanism (section 2.2) whereby in this case the precipitates are the pinning points of the dislocation line. If the applied resolved shear stress is increased further the dislocation line bows out further until the two neighboring dislocation segments meet and the opposing sides of the dislocation line annihilate. A dislocation loop is then formed around the precipitate and the dislocation line continues

to propagate through the lattice [14]. Contrary to the Frank-Read mechanism this does not lead to a source where dislocation loops are created. Also the Orowan mechanism only allows dislocations to circumvent precipitates if they are incoherent [19].

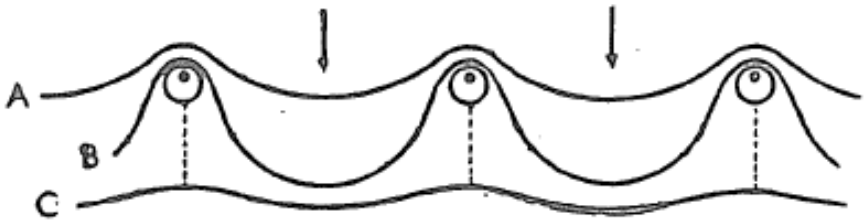

Figure 2.6: The original schematic representation of the Orowan mechanism showing the approaching dislocation line (A), the Frank-Read like bowing out of the dislocation line between the precipitates (B) and the continuation of the dislocation line (C). The circles around the dots represent the Orowan loops which are formed around the precipitates after the dislocation line has passed. Figure from: [14].

Because the bowing out of dislocations between precipitates behaves much like a Frank-Read source, the spacing between them influences the resolved shear stress needed for the dislocation line to pass the precipitates. This shear stress is given by:

$$\tau_{or} = \frac{Gb}{L_p - 2r_p} \tag{2.11}$$

where L_p is the center distance between two precipitates and r_p is the radius of the precipitate [19]. The spacing between precipitates, their volume fraction (f_p) and size are related by [19]:

$$L_p = \frac{r_p}{\sqrt{f_p}}. \tag{2.12}$$

Combining equations (2.11) and (2.12) and neglecting the $2r_p$ term because it is assumed to be small in comparison to L_p results in an expression for the shear stress based on volume fraction and radius (size). It then becomes apparent that larger precipitates provide a smaller contribution to the strength [19]

$$\tau_{or} = \frac{Gb\sqrt{f_p}}{r_p}. \tag{2.13}$$

When precipitates are passed by several dislocation lines, each line forms a dislocation loop around the precipitates. If the number of encirclements per unit volume is not too high, the resolved shear stress a dislocation line needs to pass the particles is not much higher for the next dislocation line [14]. However if the spacing between precipitates is small, the back stress exerted by the previous loop results in a high required shear stress. This means the flow stress during plastic deformation increases strongly [19]. With every loop added the effective radius of that precipitates increases, assuming that subsequent dislocation loops are not of opposing sign and annihilate. The increase in this effective radius influences the spacing through which the next dislocation can bow out and eventually circumvent the precipitate. As long as the distance between two precipitates remains large with respect to the effective radius ($r \ll L_p$), the required shear stress will increase only slightly for each additional dislocation loop.

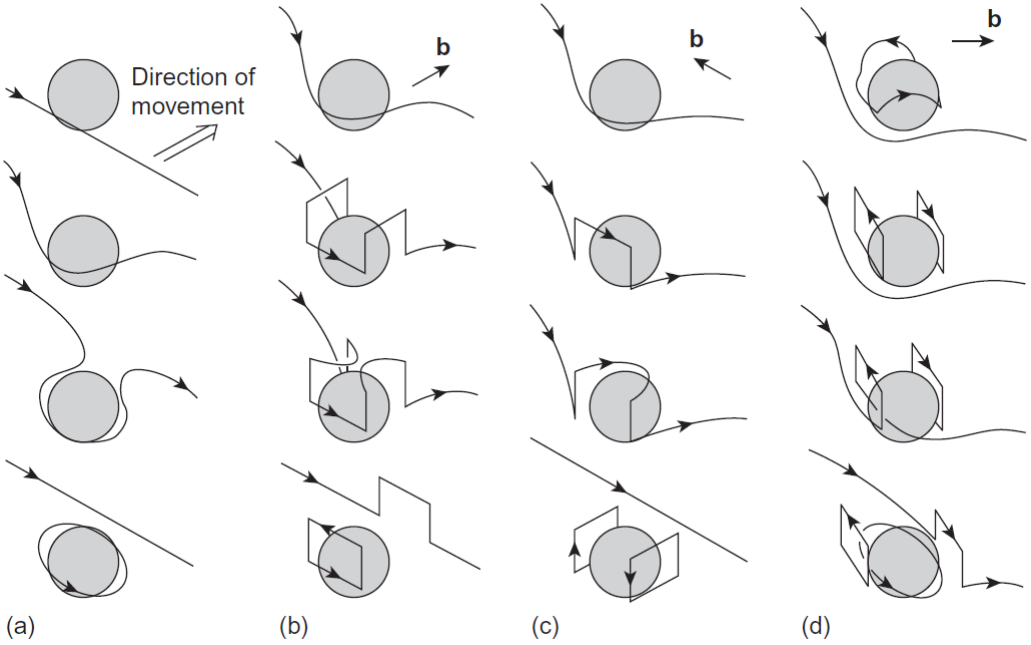

Figure 2.7: Dislocation precipitate interaction without (a) or with (b-d) cross slip. The arrow **b** indicates the orientation of the Burgers vector. (b) shows an edge dislocation passing a precipitate when cross slip occurs, (c) a screw dislocation. In (d) an Orowan loop is already present which cross slips when an additional dislocation line passes. Figure from: [15].

If the back stress on the dislocation loops becomes large enough, the dislocation loops can change their configuration and can slip on different slip systems or form prismatic dislocation loops [19]. A prismatic dislocation loop is a dislocation line which is closed inside the crystal. Its Burgers vector does not lie in the loop plane [26]. A prismatic loop does not have to be a circular loop, it can also consist of straight segments of dislocation line. Frank and Read [22] consider an edge of such loop as a potential Frank-Read source. Prismatic loops can also form as a result of the interaction between a single dislocation line with a precipitate as is shown in figure 2.7 [15]. In the formation of prismatic loops, cross slip is involved. The character of the dislocation line determines the orientation of the prismatic loop formed by the passing of a dislocation line (figure 2.7 (b) and (c)). When dislocation loops are already present around the precipitate, the passing of another dislocation line in combination with cross slip can also result in prismatic loops as well as regular Orowan loops (figure 2.7 (d)).

2.4 Dislocation behaviour in the pre-yield regime

In daily engineering practice, the yield stress of a material is most often calculated using the 0.2% strain offset, because of the absence of a clear transition in the stress-strain curve. The 0.2% offset yield criterion has however no physical meaning. Van Liempt and Sietsma [1] considered the physical yield criterion of a metal as the transition from reversible dislocation glide to dislocation multiplication. This becomes apparent in an extended Kocks-Mecking plot which plots the work hardening rate (Θ) versus the flow stress (σ), where the work hardening rate is given by:

$$\Theta = \frac{\mathrm{d}\sigma}{\mathrm{d}\varepsilon} \tag{2.14}$$

The transition from pre-yield to post-yield in the Kocks-Mecking plot, distinguished by an abrupt change in slope, represents the physical yielding of the material as indicated in figure 2.8. The 0.2% offset indicated by $R_{p0.2}$ (triangle) is in this case not equal to the physical yield stress and is underestimated. The activation of Frank-Read sources (section 2.2) is considered as the

physical mechanism for dislocation multiplication which starts the onset of plastic deformation in the physical yield criterion of van Liempt and Sietsma [1].

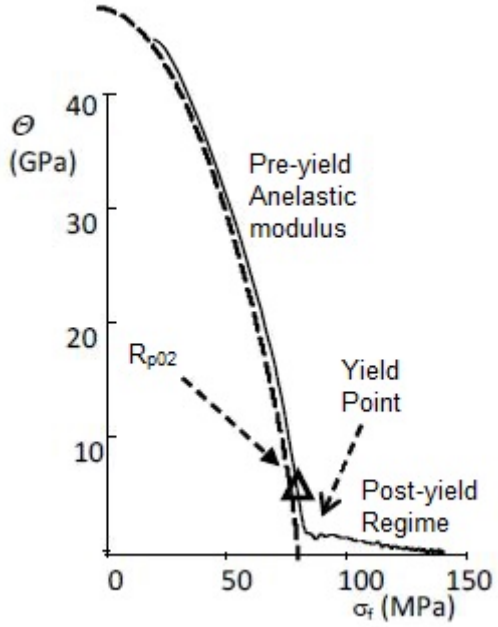

Figure 2.8: Example of an extended Kocks-Mecking plot. Phyical yielding occurs at the abrupt change of slope indicated as the yield point. The pre-yield anelastic modulus according to 2.20 is indicated by a dashed line. The 0.2% offset yield stress indicated by a triangle. Figure adapted from: [1]

In the pre-yield regime the stress-strain curve is usually presumed elastic, in accordance to Hooke's law, meaning that the deformation in this regime is reversible and proportional to the applied stress. This linear elastic behaviour is attributed to the stretching of the interatomic bonds in the lattice. The deformation in the pre-yield regime is in fact of a non-linear nature where the bowing out of dislocations, as well as other dislocation movements, also contribute to the deformation. This is referred to as anelastic deformation. Hence the total strain in the pre-yield regime can be expressed as:

$$\varepsilon_{pre} = \varepsilon_{el} + \varepsilon_{ae}, \tag{2.15}$$

where ε_{el} is the elastic strain according to Hooke's law ($\varepsilon = \sigma/E$) and ε_{ae} the anelastic contribution due to dislocation movement. Calculating the work hardening rate in the pre-yield regime by combining equations (2.14) and (2.15) leads to:

$$\Theta_{PRE} = \frac{E\Theta_{AE}}{E + \Theta_{AE}}, \tag{2.16}$$

where Θ_{AE} is the work hardening rate $\mathrm{d}\sigma/\mathrm{d}\varepsilon_{ae}$.

Van Liempt and Sietsma [1] considered the Frank-Read mechanism (section 2.2) as the sole mechanism of dislocation multiplication. Below the critical stress of the Frank-Read source the area covered by the bowing out of the dislocation line contributes to the deformation in the pre-yield regime. The shear strain introduced by the bowing out of dislocation lines is given by:

$$\gamma = \frac{\rho b A}{L}. \tag{2.17}$$

The area A was approximated by Schoeck as $A = \frac{L^3}{12r}$, which is valid for small angles of ϕ (figure 2.4) [24]. A more accurate description for the area was used by van Liempt and Sietsma by

combining equations (2.9) and (2.10) [1].

Further combination of equations (2.17), (2.9) and (2.10) leads to an expression for the strain as a function of the stress:

$$\gamma = \frac{\rho b}{L} \frac{G^2 b^2 \arcsin(\frac{\tau L}{Gb}) - GbL\tau\sqrt{1-(\frac{\tau L}{Gb})^2}}{4\tau^2}. \tag{2.18}$$

This expression can be differentiated according to $\Theta_{AE}^{\gamma} = \frac{\mathrm{d}\tau}{\mathrm{d}\gamma}$ giving the anelastic shear modulus. The critical stress of a Frank-Read source ($\tau_c = \frac{Gb}{L}$) can be combined with the term $\frac{\tau L}{Gb}$ to give a ratio of stresses $s = \frac{\tau}{\tau_c}$. Using the the Taylor factor ($\overline{M}$) the shear stress can be converted to a tensile stress by substituting $\sigma = \overline{M}\tau$ and by $\Theta_{AE} = \overline{M}^2\Theta_{AE}^{\gamma}$ the anelastic contribution becomes:

$$\Theta_{AE} = \frac{\overline{M}^2 E s^3 \sqrt{1-s^2}}{\rho L^2(1+\nu)(s - \arcsin(s)\sqrt{1-s^2})}, \tag{2.19}$$

where $s = \sigma/\sigma_c$. Substituting back in the expression for Θ_{PRE} of equation (2.16) the slope in the pre-yield regime, the pre-yield anelastic modulus, can then be expressed analytically as:

$$\Theta_{PRE} = \frac{\overline{M}^2 E s^3 \sqrt{1-s^2}}{\overline{M}^2 s^3 \sqrt{1-s^2} + \rho L^2(1+\nu)(s - \arcsin(s)\sqrt{1-s^2})}. \tag{2.20}$$

By fitting equation (2.20) to the pre-yield part of the Kocks-Mecking plot the product ρL^2 can be determined. To do so first the critical stress (σ_c) is determined graphically from the Kocks-Mecking plot by finding the stress at which Θ changes slope abruptly. However $C = \rho L^2$, where C is a constant, can be satisfied by an infinite number of combinations of ρ and L, therefore an additional equation is required. By considering a Frank-Read source of average length L, equation (2.7) can be rewritten as:

$$L = \frac{\overline{M} G b}{\sigma_c}, \tag{2.21}$$

where the Taylor factor ($\overline{M}$) is introduced to convert shear stress to tensile stress. Using the average dislocation segment length (L) the dislocation density can be deduced from the constant value obtained for ρL^2. The length obtained is an average one based on a single (macroscopic) critical stress, referred to as the physical definition of the yield stress by van Liempt and Sietsma [1]. In reality a distribution of dislocation line segments is present, each with its own microscopic critical stress [3]. A length distribution taking into account this distribution is proposed in section 2.6.

2.4.1 Applications of the physical yield criterion

The aforementioned method of finding the critical stress, as well as dislocation segment length and density has thus far only be applied on steel alloys. Van Liempt and Sietsma investigated advanced high strength steels [1]. Arechabaleta et al. investigated pure iron, a low alloy steel and interstitial free steel [3, 9]. Goulas investigated 51CrV4 spring steel [27] and Ennis et al. investigated a DP800 Dual Phase steel and TADP800 TRIP Assisted Dual Phase steel [28], as well as a DH800 dual phase steel [29]. To date no research using the physical yield criterion on other metals has been published. Because the steels that have been investigated are all predominantly BCC, it is also interesting to consider other crystal structures. The FCC crystal structure is also a very interesting candidate. The research of Kocks and Mecking was conducted predominantly using pure FCC metals [30]. Aluminium and its alloys have the FCC crystal structure. They are also common engineering materials. Some aluminium alloys are strengthened by a precipitated microstructure. Precipitate strengthening is also based on

dislocation interaction as described in section 2.3. Such a microstructure thus provides additional pinning features for the dislocations that move through the crystal. This could have effects on the results from the physical yield criterion and therefore the investigation of a precipitated aluminium alloy is of particular interest.

2.4.2 Limitations of the physical yield criterion

The yield criterion proposed by van Liempt and Sietsma [1] determines the so-called physical yield stress, average dislocation segment length and dislocation length based on the Frank-Read source as dislocation multiplication mechanism. Other mechanisms such as homogeneous nucleation, nucleation at stress concentrations, multiple cross glide, Bardeen-Herring sources and grain boundary sources [15] are not accounted for in the model. Similarly, only the contribution to the anelastic behaviour of the area swept by dislocation segments bowing out in the pre-yield regime is considered. The model also presumes that all dislocation segments are Frank-Read sources, meaning that potential Frank-Read sources which do not bow out because they are situated in non-activated slip systems are not taken into account and are therefore not included in the analysis. This means that there might be dislocations present which are not quantified which may lead errors in the obtained dislocation density. Grain boundaries also affect the behaviour of dislocation in the crystal. Van Liempt et al. [20] extended the yield criterion to incorporate grain boundary effects. These effects are not incorporated in the current model and therefore grain boundary effects are attributed to the average dislocation segment length and dislocation density. This means that the average length is not entirely due to dislocations, but also in part due to grain boundaries introducing error into the quantification of the dislocation structure. Kocks and Mecking indicate that although their experiments are performed mostly on FCC materials, that the approach is still applicable to other materials as long as they are single phase materials [30]. This holds for the post-yield regime, meaning that the analysis of the physical yield criterion could still be performed on multi-phase materials. Also an extension of the physical yield criterion taking into account different phases should be recommended.

2.4.3 The Orowan mechanism and the physical yield criterion

The introduction of incoherent precipitates in the lattice provides fixed pinning points for dislocations. These pinning points do not change their center distance as work hardening progresses apart from being subject to bulk deformation. Instead the heat treatment of the metal determines the initial size and spacing of the precipitates [19, 31]. Locks due to dislocation self-interaction do change their average distance as work hardening progresses. The result is a dislocation pinning structure which is subject to work hardening through the evolution of the dislocation structure, but also has a relatively fixed dislocation pinning structure due to precipitates when bulk deformation is neglected. The effects of such a partially fixed dislocation pinning structure on the application of the physical yield criterion model has not yet been investigated. The distance L obtained from the model is of special interest as it is the average distance between two Frank-Read source pinning points [1]. The bowing out of dislocations in a Frank-Read source and in the Orowan mechanism are described by the same set of equations [23]. The evolution of L with increased work hardening could give new insights in the hardening behaviour due to increase in dislocation density and change in dislocation structure in the lattice. When a metal is work hardened the dislocation structure in the metal changes and the length between nodes of the dislocation network decreases [3]. The rate at which L evolves with plastic strain could provide information on the influence of the precipitate structure. If L decreases only slightly when plastic strain is increased, then this could be due to precipitates at the nodes of the dislocation structure. The length between the precipitates hardly changes due to work hardening and thus the dislocation structure does not change significantly. However if the change of L is more pronounced, then the evolution of the dislocation network is most likely due to the generated dislocation loops getting stuck in the already existing network and refining the average length between nodes. These nodes would in this case most likely be dislo-

cation locks. Arechabaleta et al. investigated this work hardening behaviour using the physical yield criterion by performing interrupted tensile tests and evaluating each loading curve for the dislocation density and average segment length [3]. The investigation of a precipitated material using the physical yield criterion is thus of interest, because it could provide new insight with regard to the applicability of the yield criterion on precipitated metals, as well as possible new insights in their hardening behaviour.

2.5 Anelastic dislocation behaviour under cyclic plastic loading

When a metal specimen is loaded during a tensile test, the elastic behaviour is presumed to be linear, wheras in fact it is nonlinear (section 2.4). When the specimen is subsequently unloaded during the tensile test, its unloading behaviour is also presumed to be linear elastic in accordance with Hooke's law. This is contradictory to experimental evidence which shows that the unloading behaviour is nonlinear as well. The additional recovered anelastic strain is due to the short range reversibility of the movement of dislocations [2, 3, 8, 32].

2.5.1 Unloading and reloading behaviour

When a specimen is loaded in tension, plastically deformed and then unloaded, the final plastic strain of the specimen is often predicted by considering the elastic unloading of the specimen ($\varepsilon = \sigma/E$). If the anelastic part is not considered the plastic strain after deformation is indicated by point A in figure 2.9 whereas the experimental curve indicates a smaller final strain (point B), because strain has also been recovered due to reversible movement of dislocations. When the specimen is reloaded the tensile curve progresses as the combination of linear elastic and anelastic strain as explained in section 2.4 At point C in figure 2.9 the tensile curve crosses the unloading part of the curve and forms a hysteresis loop. Increasing the plastic deformation and repeating the unloading/reloading cycle results in another hysteresis loop. This process can be repeated until failure.

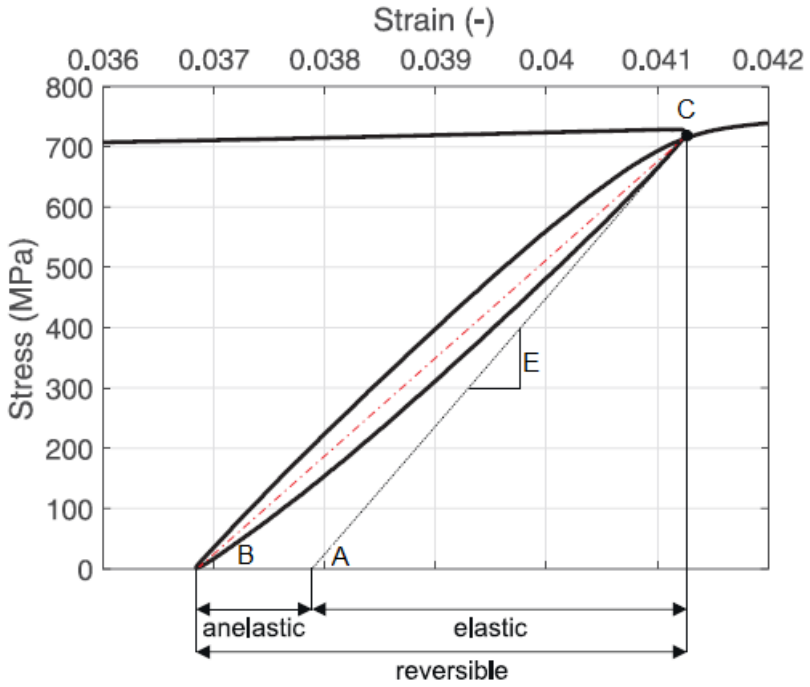

Figure 2.9: A stress-strain curve of a single unloading-reloading cycle with the E-modulus shown as a black solid line and the chord modulus as a red dashed line. The material in this figure is an AHSS. Figure adapted and based on data from Torkabadi et al. [2]

In engineering studies an approach referred to as E-modulus degradation is often applied. First the chord modulus is determined, which is given by the slope of the line crossing the lowest point of the hysteresis loop and the intersection of the unloading and reloading portion of the curve (figure 2.9 red dashed line between B and C). The chord modulus is always lower than the E-modulus, hence the term E-modulus degradation. By plastically cycling a material several times the E-modulus (in reality the chord modulus) as a function of the equivalent plastic strain can be determined. Implementing E-modulus degradation in finite element analysis improves the prediction of springback, but overestimates the springback angle [8, 32, 33]

2.5.2 Anelastic behaviour during unloading

It is presumed that a Frank-Read source which has exceeded its critical shear stress (i.e. super critical stress state) will continue to produce dislocation loops which propagate through the lattice. When the resolved shear stress is lowered from a supercritical state to a subcritical state then any loops that are currently propagating will continue to do so until impeded by obstacles in the lattice. This only happens if the magnitude of the resolved shear stress is still sufficient to accommodate slip. The required resolved shear stress, according to equation (2.6), lowers as the loop propagates further and its radius increases. So for large loops the overstress remains high and the loop propagates easily through the crystal. The new dislocation segment which was formed upon the emission of the last dislocation loop (figure 2.4 (d)), will not continue to form a loop but instead return to its equilibrium state which is determined by the applied resolved shear stress. Also any subcricital Frank-Read sources will return to their equilibrium position as the resolved shear stress decreases. The retracting Frank-Read sources thus recover anelastic strain. This makes the anelastic strain reversible across a short range proportional to the swept area of the Frank-Read source.

A constitutive model for the anelastic strain during unloading that is also based on the anelastic strain imposed by a Frank-Read source was proposed by Torkabadi et al. [2]. The model starts by considering the expression for the anelastic shear strain as function of the shear stress proposed by van Liempt and Sietsma [1] and given in equation (2.18). The relation for $s = \tau/\tau_c$ is substituted as per the physical yield criterion model to give the anelastic shear strain as:

$$\gamma = NbL^2 \frac{\arcsin(s) - s\sqrt{1-s^2}}{4s^2}. \tag{2.22}$$

The Taylor equation in its most common version:

$$\sigma_f = \sigma_0 + \overline{M}\alpha G b\sqrt{\rho}, \tag{2.23}$$

where σ_f is the flow stress and the constant σ_0 is the flow stress when no dislocations are present. Since this is never the case, Torkabadi et al. rewrote equation (2.23) to incorporate the physical yield stress (σ_y) instead. This resulted in an expression for the flow stress

$$\sigma_f = \sigma_y + \overline{M}\alpha G b(\sqrt{\rho} - \sqrt{\rho_i}) \tag{2.24}$$

which considers the increase in dislocation density with respect to the initial dislocation density ρ_i. Equation (2.24) is then written explicitly for ρ and substituted in the expression $\gamma = NbA$, where again $N = \rho/L$ and the shear strain is converted to strain by use of the Taylor factor, according to $\gamma = \overline{M}^{-1}\varepsilon$. This results in:

$$\varepsilon_{ae} = \frac{bA}{\overline{M}L}\left(\frac{\sigma_f - \sigma_y}{\overline{M}\alpha G b} + \sqrt{\rho_i}\right)^2. \tag{2.25}$$

The maximum anelastic strain that can be recovered from the material is dictated by the area covered by Frank-Read sources that have not yet passed the critical state. This means that

$A = (\pi/8)L^2$ is the maximum area determining the recoverable anelastic strain:

$$\varepsilon_{ae}^{MAX} = \frac{b\pi L}{8\overline{M}}\left(\frac{\sigma_f - \sigma_y}{\overline{M}\alpha G b} + \sqrt{\rho_i}\right)^2. \tag{2.26}$$

If the expression $\gamma_{pre} = \rho_i b A/L$ is considered, which when written explicitly for ρ_i and substituted in equation (2.26), simplifies the expression for the anelastic strain to:

$$\varepsilon_{ae}^{MAX} = \left(K(\sigma_f - \sigma_y) + \sqrt{\varepsilon_{pre}^{ae}}\right)^2 \tag{2.27}$$

where K, a fitting parameter given by:

$$K = \frac{\sqrt{b\pi L}}{\alpha G(2\overline{M})^{3/2}}. \tag{2.28}$$

2.5.3 Recovery of anelastic strain

When a metal is loaded for the first time the total strain is given by the sum of three components of strain. The elastic strain (Hooke's law, ε_{el}), the anelastic strain (reversible dislocation movement, ε_{ae}) and the plastic strain (ε_{pl}). The anelastic strain for (re)loading and unloading are considered as separate components. The total strain (ε_t) for the (re)loading case can then be expressed as:

$$\varepsilon_t = \varepsilon_{el} + \varepsilon_{ae}^{l} + \varepsilon_{pl}, \tag{2.29}$$

where ε_{ae}^{l} is the anelastic strain in the loading regime, and the plastic strain $\varepsilon_{pl} = 0$ if $\sigma < \sigma_c$. The remaining strain (ε_p) in the metal after unloading from the total strain can then be expressed as:

$$\varepsilon_p = \varepsilon_t - \varepsilon_{ae}^{ul} - \varepsilon_{el}, \tag{2.30}$$

with ε_{ae}^{ul} the anelastic strain during unloading. Equation (2.29) can be substituted in (2.30) to get the remaining strain after unloading,

$$\varepsilon_p = \varepsilon_{ae}^{l} - \varepsilon_{ae}^{ul} + \varepsilon_{pl}. \tag{2.31}$$

When the specimen is reloaded after the first cycle (loading and unloading) the remaining strain ε_p is the starting point of the subsequent cycle and should thus be added to equation (2.29). The unrecoverable anelastic strain is the difference between the anelastic strain in the loading cycle and the subsequent unloading cycle. The unrecoverable anelastic strain $\varepsilon_{ae}^{ur} = \varepsilon_{ae}^{l} - \varepsilon_{ae}^{ul}$ is used to determine the fraction of unrecoverable anelastic strain, which is given by:

$$f_{ur} = \frac{\varepsilon_{ae}^{l} - \varepsilon_{ae}^{ul}}{\varepsilon_{ae}^{l}}. \tag{2.32}$$

In the case where no plasticity is introduced into the material, the introduced anelastic strain and the recovered anelastic strain are macroscopically equal. Whether the recovered anelastic strain can be larger than the anelastic strain created during loading when plastic deformation is introduced remains unclear. To investigate this, models of anelasticity for both loading and unloading are required.

In sections 2.4 and 2.5 two models have been presented which consider the anelastic strain during loading [1], and the anelastic strain upon unloading [2]. By fitting the pre-yield anelastic modulus to an extended Kocks-Mecking plot of a loading step in the interrupted tensile curve the dislocation segment length and density can be determined. Using these two parameters the

anelastic strain can be determined according to equation (2.18) which can be rewritten for the strain by considering that $\gamma = \overline{M}^{-1}\varepsilon$, $s = \tau/\tau_c = \sigma/\sigma_c$ and $\tau_c = Gb/L$. The anelastic strain for the loading regime is then

$$\varepsilon^l_{ae} = \frac{\rho b}{L} \frac{G^2 b^2 \arcsin(\frac{\sigma}{\sigma_c}) - GbL\frac{\sigma}{\overline{M}}\sqrt{1-(\frac{\sigma}{\sigma_c})^2}}{4(\frac{\sigma}{\overline{M}})^2}. \tag{2.33}$$

The maximum anelastic strain that is introduced in the material during loading is at the critical stress of a Frank-Read source at average dislocation length, meaning that $s = \sigma/\sigma_c = 1$ and so equation (2.33) is reduced to

$$\varepsilon^l_{ae} = \frac{\pi\rho G^2 \overline{M}^2 b^3}{8L\sigma_c^2}, \tag{2.34}$$

which represents the maximum anelastic strain in the loading regime. If now the square of equation (2.21) is considered, equation (2.34) can be simplified further:

$$\varepsilon^l_{ae} = \frac{1}{8}\pi\rho L b, \tag{2.35}$$

The combination of equation (2.17) and the expression for the area of a Frank-Read source at its critical state $A = (\pi/8)L^2$ yields the same expression.

For the unloading regime the model of Torkabadi et al. using equation (2.27) can be invoked. This model has two parameters, K (equation (2.28)) and ε^{ae}_{pre}. The latter also describes the anelastic strain in the pre-yield regime, just like equation (2.34). Their expression however differs from equation (2.34). The anelastic strain as considered by Torkabadi et al. is given by $\varepsilon^{ae}_{pre} = \overline{M}^{-1}L^{-1}\rho_0 bA$, with $A = \pi L^2/8$. Although Torkabadi et al. opt to fit for K and ε^{ae}_{pre} and use these values to describe the anelastic strain of a metal, it is also possible to extract the dislocation density and length from the model. This can be done by substituting known material properties in equation (2.28) to find L and substituting it along with the other known parameter in the aforementioned equation $\varepsilon^{ae}_{pre} = \overline{M}^{-1}L^{-1}\rho_0 bA$ to find ρ_0 the initial dislocation density prior to plastic deformation. Using equations (2.34) and (2.27) the anelastic behaviour in loading and unloading can be quantified and used to determine to which extent the anelastic strain is recovered due to reversible dislocation glide.

2.5.4 Anelastic strain models and the dislocation segment length and density

Both the loading model (physical yield criterion) and the unloading model (Torkabadi et al.) use two dislocation based parameters to fit the function to the stress-strain data, the dislocation segment length L and the dislocation density ρ. The anelastic behaviour model by Torkabadi et al. does not fit to these parameters directly, but instead fits to K and ε^{ae}_{pre} from which these parameters can be calculated.

In the physical yield criterion van Liempt and Sietsma [1] used a tensile experiment where the specimens were loaded until failure and the applied stress was not interrupted in between. The model is based on the critical stress as indicated by the abrupt change of slope in the extended Kocks-Mecking plot and assumes that the dislocation structure does not change for stresses below the critical stress. Hence the model determines the dislocation density and segment length during the elastic deformation and before the subsequent plastic deformation. Torkabadi et al. [2] explicitly mention the use of the initial dislocation density and label it ρ_i to distinguish it from other dislocation densities. The dislocation length in the model is not defined explicitly as the length prior to loading. It should in fact be the dislocation length at the start of unloading which occurs after plastic deformation and thus after alteration of the dislocation structure. The expression for the anelastic strain by Torkabadi et al. considers the strain recovered based on

the area of a critical Frank-Read source. This means that the length of the dislocation segment at the start of unloading determines the expression for the anelastic strain.

In an interrupted tensile test with incremental plastic strain between each cycle, the dislocation segment length calculated using the loading and unloading model should thus differ. The decrease in dislocation segment length due to the multiplication of dislocations and the hardening because of that, should be given by the difference in length resulting from the fit of the loading and unloading models. The subsequent loading of the specimen is then expected to yield the same dislocation segment length from the fit of the physical yield criterion. In general sense this means that the dislocation segment length at the onset of yield of the n^{th} loading cycle calculated using the pre-yield anelastic modulus, should be of similar size as the dislocation segment length calculated using the constitutive model of Torkabadi et al. [2] at the $(n-1)^{th}$ unloading cycle. If this is not the case in the experimental data, further investigation on the difference between the physical yield criterion model and the constitutive model with respect to the dislocation segment length is required.

2.6 Dislocation segment length distribution

The physical yield criterion assumes that all Frank-Read source segments are of equal length. The segment length is however distributed and the length L in equation (2.21) is an average of of all dislocation line segments represented in the dislocation density. By means of equation (2.21) it becomes apparent that the longest dislocations will yield first and thus the onset of yielding is governed by the longer dislocations. The mechanical behaviour of crystalline metals can be better understood by considering a dislocation segment length distribution [3]. Therefore it is of specific interest to characterize the effects of a dislocation segment length distribution. Upon plastic deformation the dislocation structure also becomes more heterogeneous [34]. A cell structure forms with regions of high and low dislocation density. Meaning that the evolution of the dislocation structure might also influence the distribution of the dislocation line segment lengths inside the crystal . Therefore the analysis of the evolution of the dislocation structure by plastically cycling material and intermediate evaluation of the structure could be of particular interest. In this section a continuous uniform distribution model for the dislocation length is proposed, whereby the box is centred on the long side of the length range (see figure 2.10). The benefit of using a box type distribution is that an analytical solution can be obtained. This distribution presumes that each dislocation segment length has the same density in the metal.

2.6.1 Distributed dislocation length and the physical yield criterion

Prior to the introduction of the continuous uniform dislocation line segment distribution equation (2.20) is rewritten as

$$\Theta_{PRE}(s) = \frac{E}{1+\frac{(1+\nu)}{\overline{M}^2}\rho L^2\left(\frac{s-\arcsin(s)\sqrt{1-s^2}}{s^3\sqrt{1-s^2}}\right)} = \frac{E}{1+V\rho L^2 S(s)}. \tag{2.36}$$

To simplify equation (2.36) the stress dependent part of Θ has been written as $S(s)$ a function of s. Additionally a constant term $V = (1+\nu)/\overline{M}^2$ can be identified to simplify equation (2.36) further. Subsequently a normalization $T_{ND} = \Theta(s)/\Theta(0)$ can be applied, where $\lim_{s\to 0}\Theta(s) = \frac{1}{3}$ resulting in the following expression for T_{ND}:

$$T_{ND} = \frac{1+\frac{V}{3}\rho L^2}{1+V\rho L^2 S(s)}. \tag{2.37}$$

In the expression for T_{ND}, the normalized non-distributed pre-yield anelastic modulus, the Young's modulus is eliminated and T_{ND} can now be plotted as function of s to obtain a normalized Kocks-Mecking plot with no segment length distribution as shown in figure 2.11.

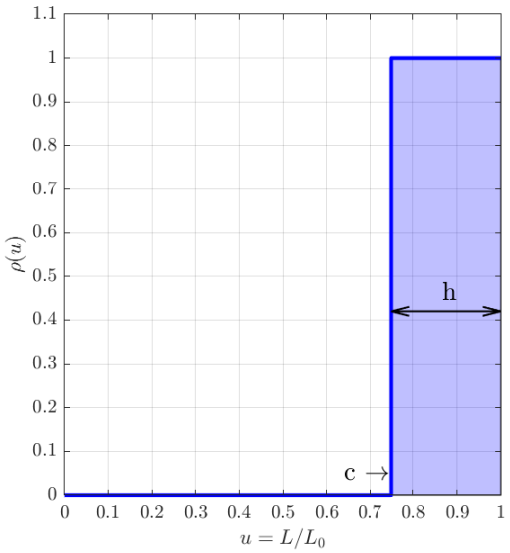

Figure 2.10: Continuous uniform distribution fixed at the right side at the maximum dislocation length. The box is defined by the width h.

Subsequently a box type distribution for the dislocation segment length can be implemented by considering the integral of the distribution from c to 1 and introducing it in equation (2.37). The dislocation length is normalized by taking $u = L/L_0$ with L_0 the length of the longest dislocation line segment that yields first indicated by the abrupt change of slope in the extended Kocks-Mecking plot, resulting in the expression:

$$T_D = \frac{1 + \frac{VL_0^2}{3}\rho(u)\int_c^1 u^2 \mathrm{d}u}{1 + VL_0^2\rho(u)\int_c^1 u^2 \frac{su - \sqrt{1-(su)^2}\arcsin(su)}{(su)^3\sqrt{1-(su)^2}}\mathrm{d}u}. \tag{2.38}$$

Here $s = \sigma/\sigma_{c0}$, with σ_{c0} the critical stress at the maximum dislocation length L_0. The analytical solution of the integral in the numerator is ($\int_c^1 u^2 \mathrm{d}u = \frac{1}{3} - \frac{c^3}{3}$). The integral in the denominator has a slightly more complex analytical solution which is given by:

$$I_\rho(c,s) = \int_c^1 \rho(u) u^2 \frac{su - \sqrt{1-(su)^2}\arcsin(su)}{(su)^3\sqrt{1-(su)^2}}\mathrm{d}u = \rho(u)\left[\frac{\arcsin(su) - \arcsin(su)\ln(1 - e^{2\mathrm{i}\arcsin(su)}) + \frac{1}{2}\mathrm{i}(\arcsin(su)^2 + \mathrm{Li}_2(e^{2\mathrm{i}\arcsin(su)}))}{s^3}\right]_c^1, \tag{2.39}$$

$\rho(u)$ is moved outside the integral in equation (2.38). This is allowed because for a uniform distribution $\rho(u)$ is a constant. The two integrals are evaluated and subsequently substituted in equation (2.38). The expression is further normalized by the introduction of ρ_0 the dislocation density which is assumed the same for all segment lengths. It equals $\rho_0 = \rho(u)\int_c^1 u^2 \mathrm{d}u$. Further normalization is realized by dividing the evaluated integrals to arrive at:

$$T_D = \frac{1 + \frac{V}{3}\rho_0 L_0^2}{1 + V\rho_0 L_0^2 \frac{I_\rho(c,s)}{\frac{1}{3} - \frac{c^3}{3}}}. \tag{2.40}$$

The total width of the box in the continuous uniform distribution (h) can be introduced into equation (2.40) as $c = 1 - h$. This approach provides an additional fitting parameter (h) to the physical yield criterion which can be used to fit the model more accurately to the data obtained from derivative of the tensile curve.

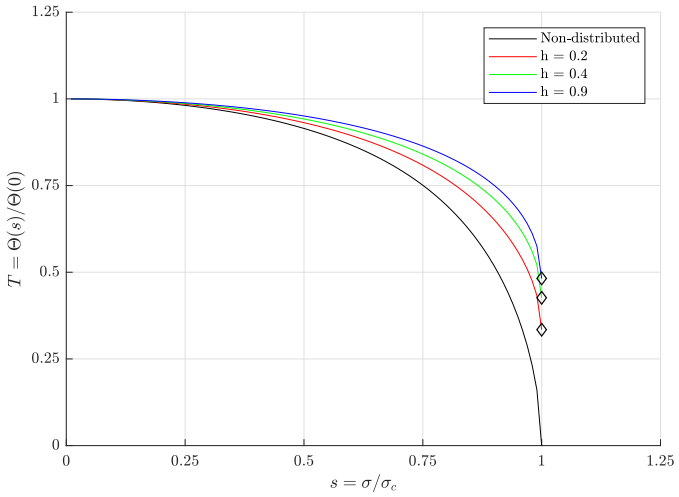

Figure 2.11: Normalized Kocks-Mecking plot without a distribution (T_{ND}) with $\rho L^2 = 10$, an arbitrary but realistic value. The introduction of the distribution model (T_D) shows that T_D at $s = 1$ is no longer 0 but instead lifts up as the width of the distribution increases.

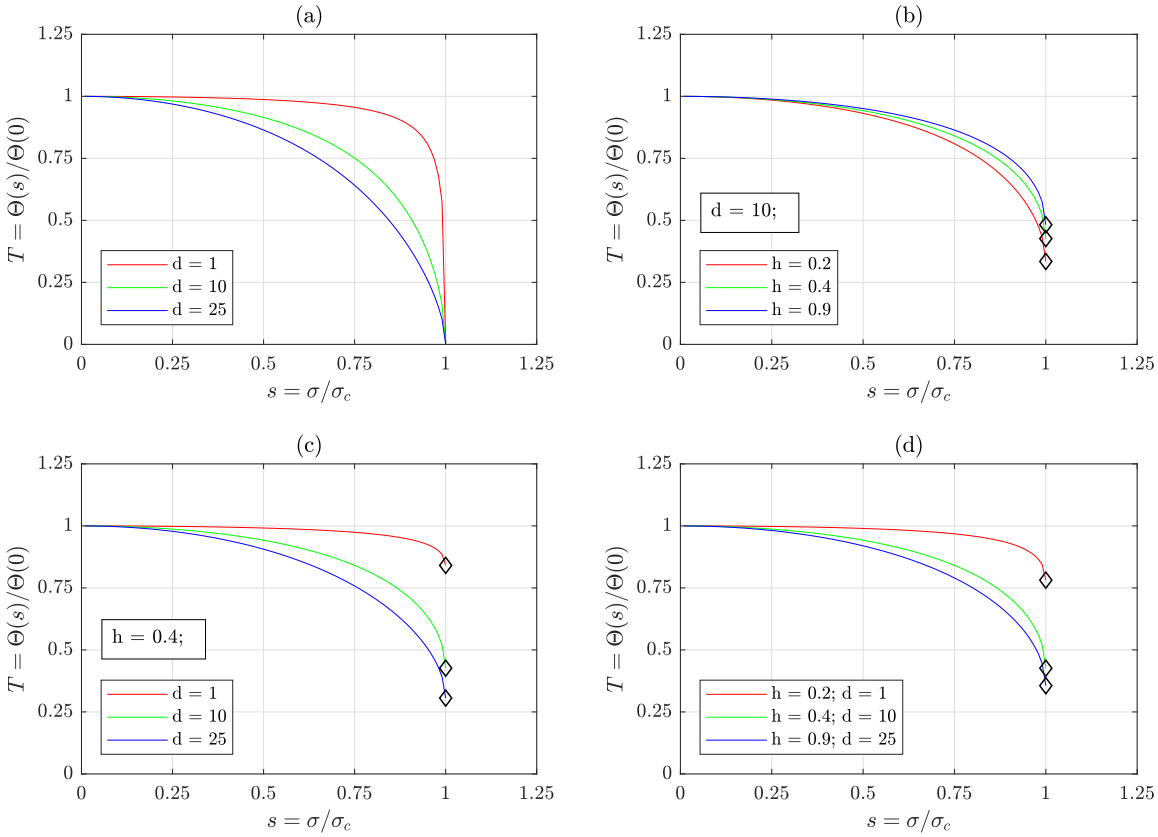

Figure 2.12: Effects of the parameters h and $d = \rho_0 L_0^2$. (a) The effect of d on the T_{ND} curve. (b) The effect of the continuous uniform distribution width (h) on the value of Θ_c. (c) The effects of d on the value of Θ_c in the distributed model. (d) The combined effects of h and d on the shape of the T_D curve and the value of Θ_c.

2.6.2 Influence of the length distribution on the anelastic pre-yield behaviour

The influence of the fitting parameters ρ_0, L_0 and h is presented in figure 2.12. The parameters ρ_0 and L_0 are combined for convenience, in the symbol $d = \rho_0 L_0^2$. When T_D is plotted for different values of h (figure 2.11) it becomes apparent that the width of the box affects the value T_D at $s = 1$. A larger value for h results in a higher value of T_D. This behaviour implies that the value for Θ_c ($\diamond$) can be related to the distribution of dislocation segment lengths.

The parameter d dictates the shape of the curve of the non-distibruted pre-yield anelastic modulus T_{ND} (equation (2.37)), as can be seen in figure 2.12 (a). This effect carries over to the distributed model as well, according to equation (2.40). As d goes to 0, T becomes 1 throughout the range s (figure 2.12 (c)). This is in agreement with purely linear elastic behaviour without any anelastic dislocation interaction [1]. However the value of Θ_c is then also influenced by d, where a reduction of d results in an increase of Θ_c as can be seen in figure 2.12 (c). The width of the continuous uniform distribution also changes the value of Θ_c. An increase in h results in an increase of Θ_c. The influence on the shape is far less pronounced in comparison to the effects of d.

2.7 Summary

The reversible movement of dislocation causes a non-linear elastic strain prior to the yield of the material. The critical stress, or physical yield stress, is graphically determined in an extended Kocks-Mecking plot, in which it can be observed as an abrupt change of slope. Van Liempt and Sietsma developed a method to obtain the dislocation density and average dislocation segment length from the pre-yield regime of the extended Kocks-Mecking plot using the pre-yield anelastic modulus [1]. This method has thus far only been used on steels, therefore the investigation of an face centred cubic metal such as aluminium is of interest. The use of aluminium also allows for the introduction of precipitates which form stationary pinning points, which do not move when work hardening is introduced. Also the influence of precipitates on the dislocation density and dislocation structure can become apparent after tensile testing. The downside of the model is that other mechanisms of multiplications and dislocation segments on non-activated slip planes are not considered. Grain boundary effects are not accounted for either. The length resulting from the fit of the pre-yield anelastic modulus to the extended Kocks-Mecking plot is an average dislocation segment length. In order to account for a length distribution in the dislocation structure a continuous uniform distribution was added onto the existing model. This gives an additional parameter h, which represents the width of the box distribution.

During unloading the dislocation segments also provide an anelastic component to the unloading behaviour. Torkabadi et al. [2] developed a constitutive model for unloading closely related to the model by van Liempt and Sietsma [1]. The fitting parameters of the constitutive model also include the dislocation density and average segment length, albeit indirectly. By performing interrupted tensile tests with incremental strain, both these models can be tested to investigate whether they return the same densities and lengths. This interrupted tensile testing will give information on the evolution of the dislocation density and segment length with plastic strain. The two models, for loading and unloading, potentially also enable the investigation of the amount of recovered anelastic strain.

CHAPTER 3

Experimental Details

An AA7075 aluminium alloy was used for the investigation on the effects of a precipitated microstructure on dislocation behaviour during anelasticity. AA7075 is a Al-Mg-Zn based alloy which properties can be influenced by precipitation hardening, this process is also referred to as age-hardening. After a solution heat treatment the atoms of the alloying elements are in Super Saturated Solid Solution (SSSS). During precipitation hardening incoherent η ($MgZn_2$) precipitates grow from Guinier-Preston (GP) zones followed by the semi-coherent η' phase (SSSS $\rightarrow$ GP $\rightarrow \eta' \rightarrow \eta$). This happens during an an artificial ageing heat treatment at a lower, yet still elevated temperature. The temperature determines the extent to which the alloying elements can diffuse through the aluminium lattice to form precipitates. The incoherency of the precipitates means that they cannot be sheared, but only circumvented by for instance the Orowan mechanism (section 2.3). The spacing of the precipitates is independent from the work hardening of the material during plastic deformation. This means that the precipitates form pinning points for dislocations that do not change during work hardening [19, 31].

Two types of mechanical tests were performed, first conventional tensile tests to validate the applicability of the physical yield criterion on aluminium and AA7075 and to obtain data to fit the new distributed segment length model. These tests also result in the physical yield stress of the aluminium and the aluminium alloys after different heat treatments. Second, interrupted tensile tests were performed to investigate the evolution of dislocation density, dislocation segment length and the recovery of anelastic strain during plastic deformation. These test were performed in similar manner as in [3] and were fitted with the models presented in section 2.4 and 2.5 on the loading and unloading curves of the interrupted tensile test respectively.

3.1 Materials

Two types of metals were used in the experimental work, a pure aluminium (99.9%) and the commercial AA7075 alloy which was supplied in two batches, labelled A and B respectively. Specimens were made from 8 mm diameter wire (aluminium) and rod (AA7075) and heat treated prior to the experiments. The specimens were machined to final dimensions after the heat treatment according to figure 3.1 (a) or (b) depending on the test.

3.1.1 Chemical compositions

The chemical composition of AA7075 in batch A and B was analysed using X-ray Fluorescence (XRF) spectrometry. The analysis was performed using a Panalytical Axios Max WD-XRF spectrometer and data evaluation was done with SuperQ5.0i/Omnian software. The resulting chemical compositions are presented in table 3.1 along with the theoretical composition. The supplied aluminium wire had a purity of 99.9%. The solute elements in the aluminium were not further investigated.

Table 3.1: Theoretical chemical composition (T) of AA7075 [35] and the chemical composition (wt.%) of batch A and B from XRF-analysis.

	Si	Fe	Cu	Mn	Mg	Cr	Zn	Zr	Ti	other	Al
T	0.40	0.50	1.2-2.0	0.30	2.1-2.9	0.18-0.28	5.1-6.1	0.25%[1]	0.20	0.15[2]	bal.
A	0.207	0.241	1.712	0.101	2.514	0.162	5.29	-	0.06	0.079[3]	89.632
B	0.22	0.29	1.678	0.096	2.536	0.206	5.094	-	0.073	0.062[4]	89.717

[1] A maximum of 0.25% of (Zr + Ti) may be used.
[2] A maximum of 0.05 wt% of an single element may be present, accumulating to a total of 0.15.
[3] Other elements: 0.04 Pb, 0.018 Cl, 0.011 P and 0.01 Ni.
[4] Other elements: 0.033 Pb, 0.019 Cl and 0.01 Ni.

3.1.2 Heat treatments

All AA7075 specimens were subjected to a solution treatment at 470 °C for 1 hour in a sodium nitrite bath, followed by a water quench to room temperature. Subsequently an ageing treatment in silicon oil was conducted at 120 °C for 0, 16, 24 and 32 hours after which specimens were air cooled to room temperature. The 24 hour ageing heat treatment at 120 °C is equivalent to commercial AA7075-T6 [35].

The aluminium samples were also heat treated at 470 °C for 1 hour in a sodium nitrite bath. Half of the specimens were left to air cool to room temperature whereas the other half was water quenched to room temperature.

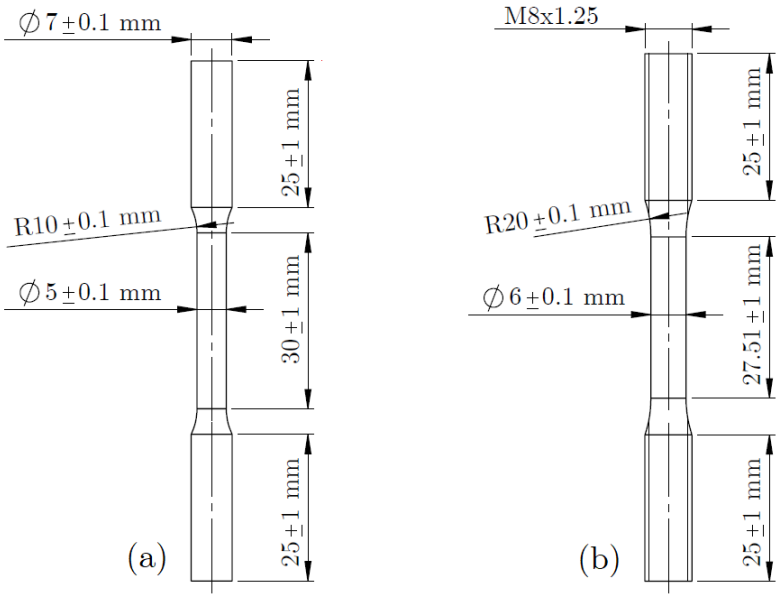

Figure 3.1: Specimen dimensions for the conventional tensile test (a) and the interrupted tensile test (b).

3.2 Method

Two types of mechanical tests were performed. A tensile test to determine the physical yield stress, dislocation density and average segment length were performed first. Next, interrupted tensile tests with incremental plastic strain between each cycle were performed. The reloading after plastic deformation allows for quantification of dislocation density, average segment length as a function of the induced plastic strain.

3.2.1 Equipment

Tensile and cyclic tests were conducted on a Instron 5500R Universal Testing Machine. During the tensile test the machine was equipped with a 100 kN load cell and wedge grips and operated at a crosshead speed of 10 mm/min which corresponds to a measured strain rate of 0.0017 s^{-1}. Dual extensometers were mounted on opposing sides of the narrow section of the specimen. The extensometers were removed at 10% strain for the aluminium samples and at 5% for the AA7075 samples.

During the interrupted tensile tests the specimens were mounted in threaded inserts which were connected directly to flanges mounted on the load cell and the crosshead. The connection between the threaded inserts and the play on the thread allowed for some self aligning movement of the specimen. Again two extensometers were mounted on opposing sides of the narrow section of the specimen. The specimens were loaded in extension control at a crosshead speed of 1 mm/min which corresponds with a measured strain rate of 0.015 s^{-1}. Loading continued until 1% strain was reached. The strain used to control the cyclic behaviour was measured on only one of the two extensometers. Subsequently the specimens were unloaded to 100 N ($\approx$ 3.3 MPa) at the same crosshead speed. The specimen was then reloaded and another 1% strain was introduced. This loading-unloading-reloading was repeated with 1% increments of strain until failure of the specimen.

CHAPTER 4

Results

The results of the tensile tests and interrupted tensile tests are presented, results from the analysis according to the physical yield criterion (section 2.4) and the constitutive unloading model by Torkabadi et al. [2] (section 2.5) are also presented. First the tensile tests results are discussed, followed by the results of the interrupted tensile tests.

The parameters used in the pre-yield anelastic modulus derived in the physical yield criterion model, but not designated as fitting parameters are shown in table 4.1. The shear modulus (G) is calculated from the Young's modulus (E) and the Poisson's ratio (ν). The Burgers vector (b) is calculated from the lattice parameter (a) according to: $b = a\sqrt{h^2 + k^2 + l^2}$, where h, k and l are the Miller indices of the dislocation glide planes in the FCC crystal structure. The Taylor factor ($\overline{M}$), the Poisson's ratio and the Young's modulus are obtained from literature. For the Young's modulus literature values based on ultrasonic experiments were used as the motion of dislocation and thus their contribution to the Young's modulus can be neglected [36].

Table 4.1: Physical constants used in the physical yield criterion model.

Parameter	Aluminium	AA7075	Units	Ref.
$\overline{M}$	3.06	3.06	[-]	[37]
ν	0.339	0.33	[-]	[38] & [39]
E	69.6×10^3	69.4×10^3	MPa	[38] & [39]
$G = \frac{E}{2(1+\nu)}$	25.9×10^3	26×10^3	MPa	[38] & [39]
b	2.863	2.866	Å	[40, 41] & [42]

4.1 Tensile tests results

The results from the tensile tests and the subsequent analysis according to the physical yield criterion are listed in table 4.2. Results are presented for pure aluminium and AA7075 independently.

4.1.1 Tensile testing results - Pure Al

The results of the tensile tests on quenched and air cooled pure aluminium and the physical yield criterion analysis are listed in table 4.2. The extended Kocks-Mecking plots are presented in figure 4.1. The air cooled (AC) aluminium shows no real curvature in the pre yield regime. The fitting of the physical yield criterion model to the data was poor, resulting in data for the dislocation density and average segment length that are not representative. A change of slope is still apparent in the Kocks-Mecking plot, this change is however not as abrupt as the quenched specimen which leaves room for error in the determination of the physical yield stress of the pure aluminium. The fit of the pre-yield anelastic modulus to the data of the quenched aluminium specimen is shown in figure 4.1.

Table 4.2: $R_{p0.2}$ yield stress ($\sigma_{R_{p0.2}}$), physical yield stress (σ_c), dislocation density (ρ) and average segment length (L) of AA7075 heat treated at 0, 16, 24 and 32 hours. The standard error for all stress values is ± 1 MPa.

2^{nd} Heat treatment	Material (Batch)	$\sigma_{R_{p0.2}}$ [MPa]	σ_c [MPa]	ρ [m^{-2}]	L [nm]
none	AA7075 (A)	366	368	$6.50 \pm 0.03 \times 10^{14}$	61.9 ± 0.13
none	AA7075 (B)	349	346	$5.37 \pm 0.02 \times 10^{14}$	65.9 ± 0.13
16 h / 120 °C	AA7075 (A)	557	556	$1.127 \pm 0.006 \times 10^{15}$	41.0 ± 0.13
16 h / 120 °C	AA7075 (B)	551	550	$1.022 \pm 0.006 \times 10^{15}$	41.4 ± 0.13
24 h / 120 °C	AA7075 (A)	517	515	$1.42 \pm 0.01 \times 10^{15}$	44.3 ± 0.14
24 h / 120 °C	AA7075 (B)	575	572	$1.07 \pm 0.01 \times 10^{15}$	39.8 ± 0.15
32 h / 120 °C	AA7075 (A)	583	582	$1.32 \pm 0.01 \times 10^{15}$	39.2 ± 0.15
32 h / 120 °C	AA7075 (B)	576	579	$1.69 \pm 0.01 \times 10^{15}$	39.4 ± 0.15
Air cooled	Al (99.9%)	37	27†	$7.7 \pm 0.6 \times 10^{13}$	857.1 ± 0.12
Quenched	Al (99.9%)	52	52	$6.446 \pm 0.003 \times 10^{13}$	443.6 ± 0.09

† No abrupt change of slope was observed in the Kocks-Mecking plot.

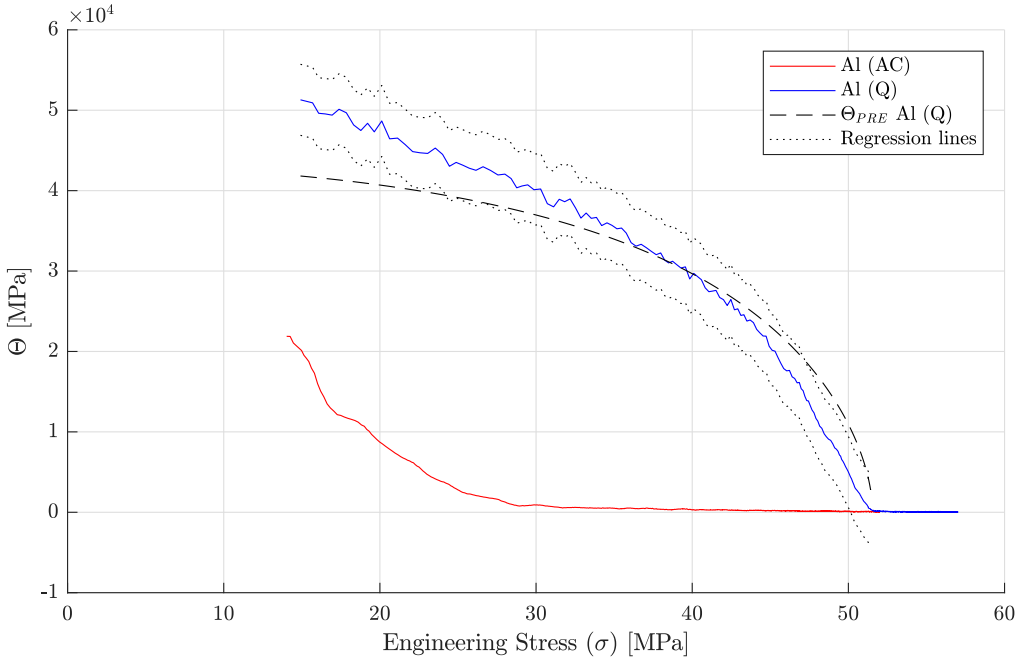

Figure 4.1: Extended Kocks-Mecking plot of aluminium, air cooled (AC) and quenched (Q). The air cooled aluminium shows a gradual change of slope in comparison to the rather abrupt change observed for the quenched specimen. The curvature of the pre-yield regime of the pure aluminium specimen could not be used to fit equation (2.20).

4.1.2 Tensile testing results - AA7075

The AA7075 specimens in the tensile tests were subjected to four different heat treatments, first a solution treatment, followed by age-hardening treatments at 0, 16, 24 and 32 hours as discussed in section 3.1.2. As expected the specimens at 0 hours have a much lower yield stress. The effect of age-hardening becomes apparent in the shift to the left of the point where the slope of each curve changes abruptly. More results are given in table 4.2. All specimens failed in a brittle manner with a fracture along a plane inclined 45° to the tensile axis. A minimal amount of necking preluded the failure of the specimens.

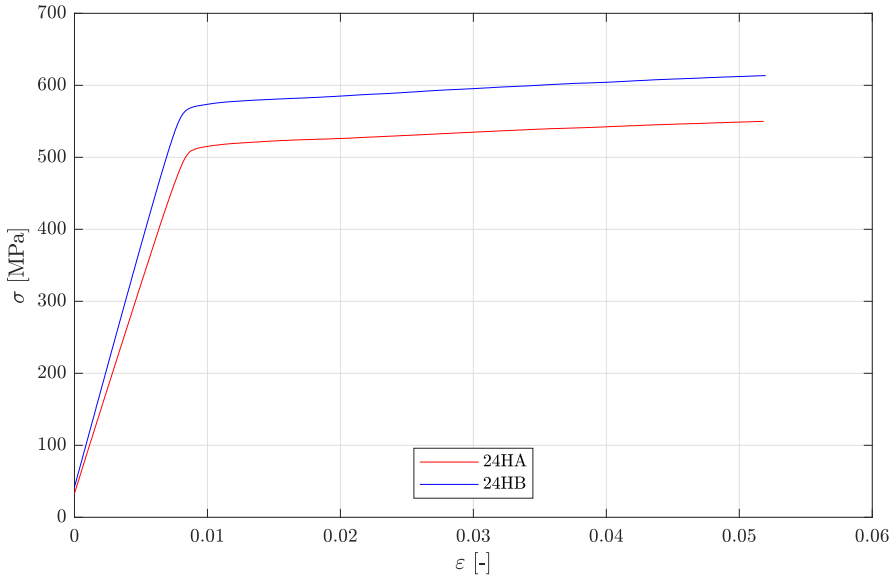

Figure 4.2: A stress-strain curve of AA7075 specimens aged for 24 hours from batch A and B. The specimen from batch A has a more gradual slope in the pre-yield regime and a lower yield stress. This is also apparent in the extended Kocks-Mecking plot in figure 4.3.

The plateau at low stresses in figure 4.3, related to the Young's modulus of the alloy, stands out in the case of the specimen from batch A aged at 24 hours. Also the yield stress of this specimen is lower than that of a specimen of similar heat treatment from batch B. The stress-strain curves of specimens 24HA and 24HB presented in figure 4.2 show a more gradual slope in the pre-yield regime for specimen 24HA. The gradual slope is directly related to the plateau value in figure 4.3. The yield stress is also lower, which is also apparent from figure 4.3. The clamped surfaces of the specimen were investigated, but no visual evidence of slip inside the wedge grips was found. The strain rate (0.0011 s^{-1}) of the specimen was however lower than most other specimens (0.0018 s^{-1}). The crosshead displacement data was constant and corresponded with other experiments, providing no direct explanation for the deviation in material properties.

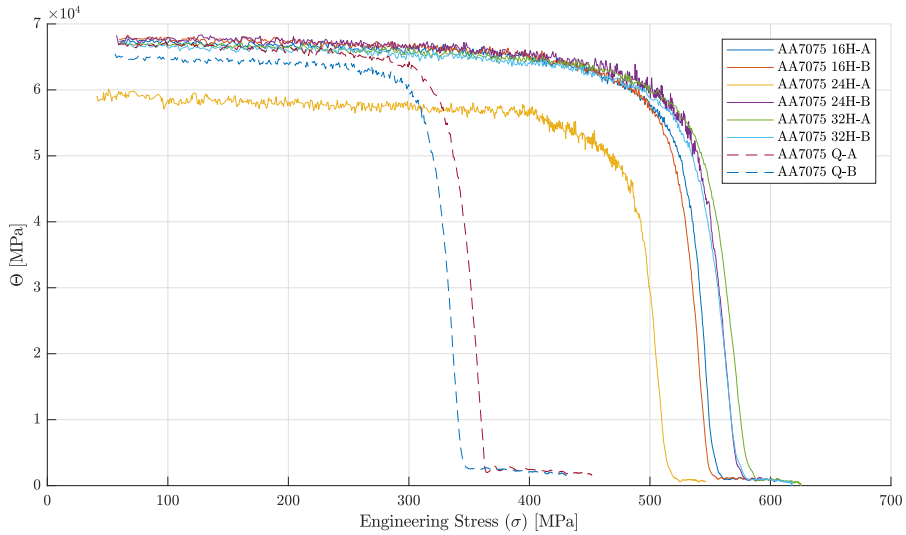

Figure 4.3: Extended Kocks-Mecking plot derived from tensile tests of AA7075 specimens from batch A and B heat treated at 0, 16, 24 and 32 hours after a solution heat treatment.

Figure 4.4 shows the physical yield stress (σ_c) and the 0.2% strain offset yield stress ($\sigma_{R_{p0.2}}$) as a function of the age-hardening heat treatment time. The drop for the 24 hours specimen from batch A is clearly apparent as explained previously. The difference between σ_c and $\sigma_{R_{p0.2}}$ is small, meaning that for AA7075 the physical definition of the yield stress and the classical 0.2% strain offset yield stress are in good agreement. As the age-hardening time increases the yield stress appears to approach a maximum. The specimens heat treated for 24 hours should be in the peak hardened state (T6) [35]. This is however not the case as the specimens heat treated for 32 hours exhibit a still higher yield stress.

The influence of the age-hardening heat treatment time on the dislocation density (ρ) and the average segment length (L) is depicted in figure 4.5. The average dislocation segment length shows similar behaviour as σ_c in figure 4.4, including an increase in L for the 24HA specimen. This similarity was expected as the dislocation segment length is obtained using the relation in equation (2.21), which is dependent on the critical stress. The dislocation density increases as the age-hardening heat treatment time increases. Figure 4.5 shows some unexpected behaviour at higher age-hardening times, where the dislocation density in batch A suddenly decreases at 32 hours, whereas the specimen from batch B shows a drop at 24 hours. The dislocation density does not show particular resemblance to the yield stress plotted in figure 4.4 because of the dependence on the curvature of the extended Kocks-Mecking plot rather than a single value like the critical stress.

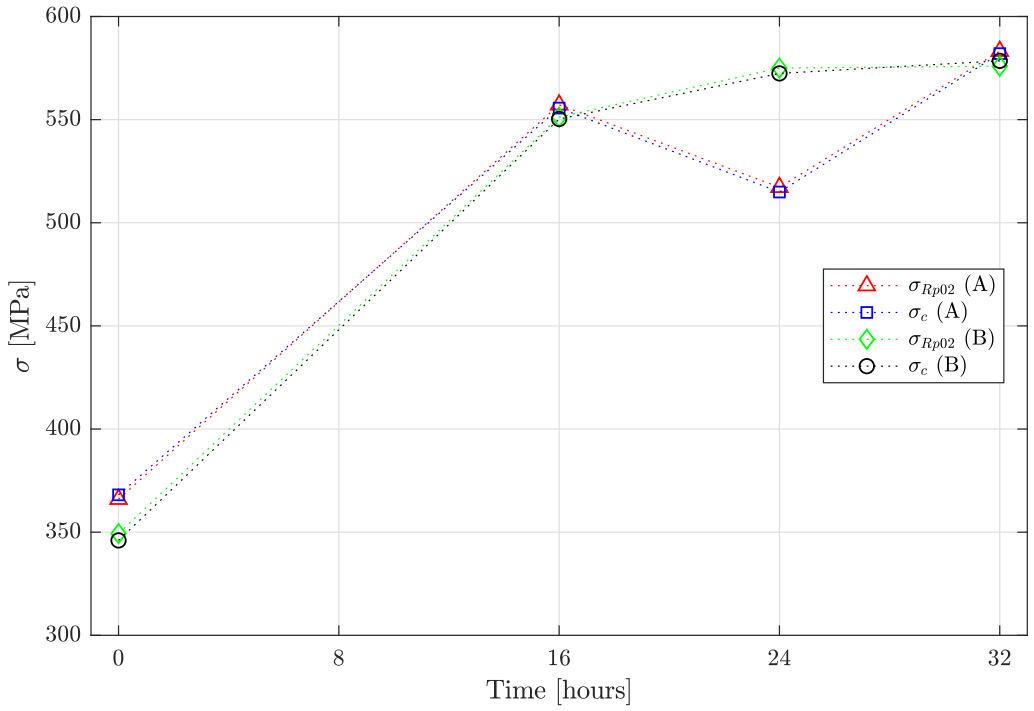

Figure 4.4: Physical yield stress (σ_c) and 0.2% strain offset yield stress ($\sigma_{R_{p02}}$) of AA7075 (batch A and B) as function of the age-hardening time (0, 16, 24 and 32 hours). Standard errors for the stress are $\pm$ 1 MPa.

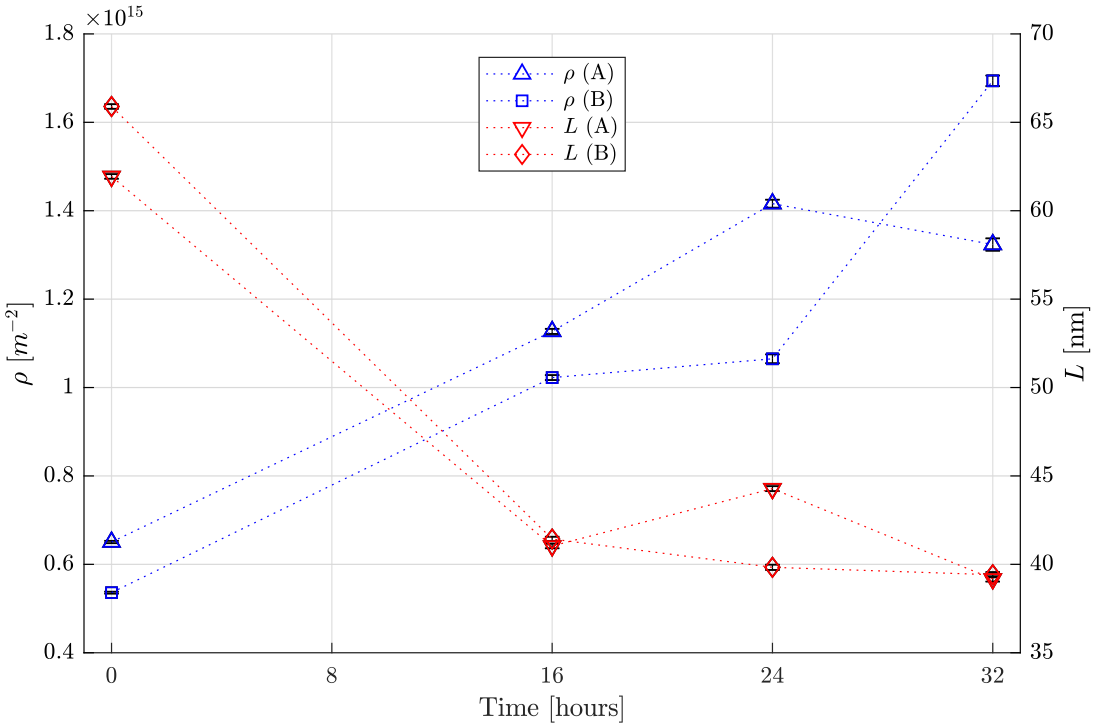

Figure 4.5: The dislocation density and average dislocation segment length of AA7075 (batch A and B) as function of the age-hardening time (0, 16, 24 and 32 hours).

4.1.3 Dislocation segment length distribution - AA7075

The normalized distributed pre-yield anelastic modulus (equation (2.40) in section 2.6) was fitted to the normalized extended Kocks-Mecking plot derived from the tensile data. The continuous uniform distribution of the dislocation segment length introduced into the normalized pre-yield anelastic modulus provides an additional fitting parameter (h) which represents the width of the box in the distribution. The results of such a fit, plotted in figure 4.6, show no clear distinction from the regular normalized fit at first glance. However a close-up (figure 4.7) reveals that $T_D(1) = 0.0075$ a positive value which lifts the end of the anelastic pre-yield model into the vicinity of the abrupt change of slope. The corresponding width of the continuous uniform distribution (figure 2.10) is then $h = 1.7 \times 10^{-5}$. Results from the other specimens are listed in table 4.3.

Table 4.3: Dislocation density (ρ), average segment length (L) and the width of the box in the continuous uniform distribution (h) of AA7075 from batches A and B heat treated at 0, 16, 24 and 32 hours.

	0h(A)	0h(B)	16h(A)	16h(B)	24h(A)	24h(B)	32h(A)	32h(B)
ρ [m^{-2}] ($\times 10^{15}$)	1.17	1.15	2.19	2.07	2.90	2.11	3.041	3.08
L [nm]	62.5	65.8	41.7	41.4	44.2	39.8	39.1	39.6
h [-] ($\times 10^{-5}$)	2.3	4.6	0.04	0.8	2.3	1.7	1.2	1.1

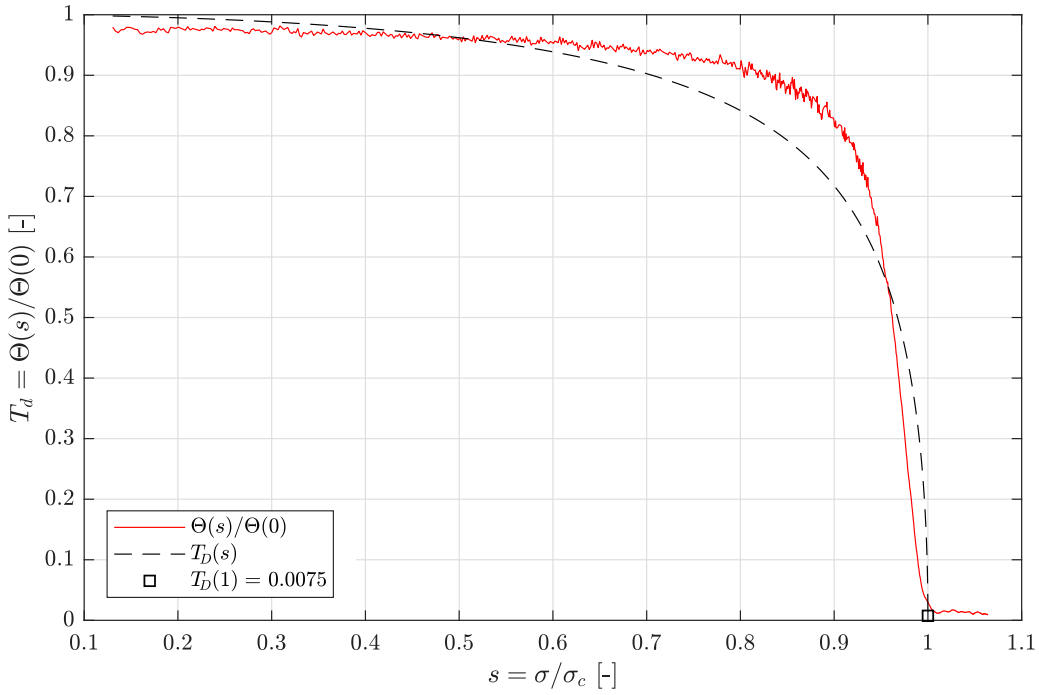

Figure 4.6: A normalized extended Kocks-Mecking plot fitted with the distributed model from equation (2.40). The specimen shown was aged for 24 hours and was taken from batch B. The distributed model does not end at $T_D(1) = 0$ as can be seen in figure 4.7.

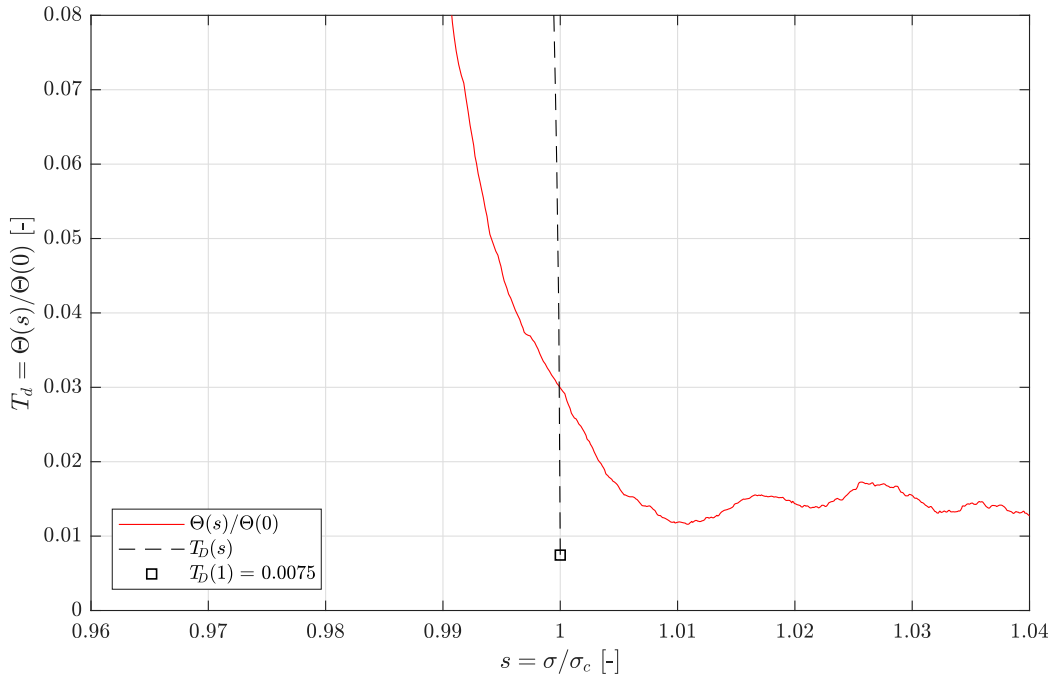

Figure 4.7: Close-up of $T_D(1)$ from figure 4.6 showing that at $s = 1$, $T_D(1) \neq 0$ but is instead a positive value.

4.2 Interrupted tensile tests

Interrupted tensile tests were conducted, whereby after each cycle the strain was increased by 1%. A typical result of such an interrupted tensile test is shown in figure 4.8. Cycles were defined between the local minima and maxima of strain. One of the strain gauges was used to monitor the strain during the test which determined when the (re)loading cycle ended. Figure 4.8 shows however the average strain and as such the cycles do not stop at exactly a multiple of 1%. Also the last cycle was neglected because of the failure of the specimen in this cycle. The reloading cycles, following the primary loading cycle, exhibit peaks at the beginning of plastic deformation where the stress decreases before gradually increasing again. This phenomena appeared in each specimen. The strain rate and crosshead displacement were investigated. The rate of displacement of the crosshead was constant and the strain rate increased at the onset of plastic deformation, which indicates multiplication of dislocations. So neither can explain the bulges at the start of the post-yield regime.

4.2.1 Results of the interrupted tensile tests

An extended Kocks-Mecking plot was constructed for each loading cycle, typical results are shown in figure 4.9. As the number of cycles increases, the plateau of the extended Kocks-Mecking curve lowers slightly and the stress at which the slope changes abruptly increases. Identification of this slope is not as straightforward as with the regular tensile tests because the stress bulges at the onset of plastic deformation cause the Kocks-Mecking curve to spiral around as can be seen in figure 4.9. The severity of the spiralling near the critical stress is dependent on the shape of the bulge in the tensile curve. A narrower bulge causes larger spiralling. Nonetheless the physical yield stress, dislocation density and average segment length were determined for each cycle.

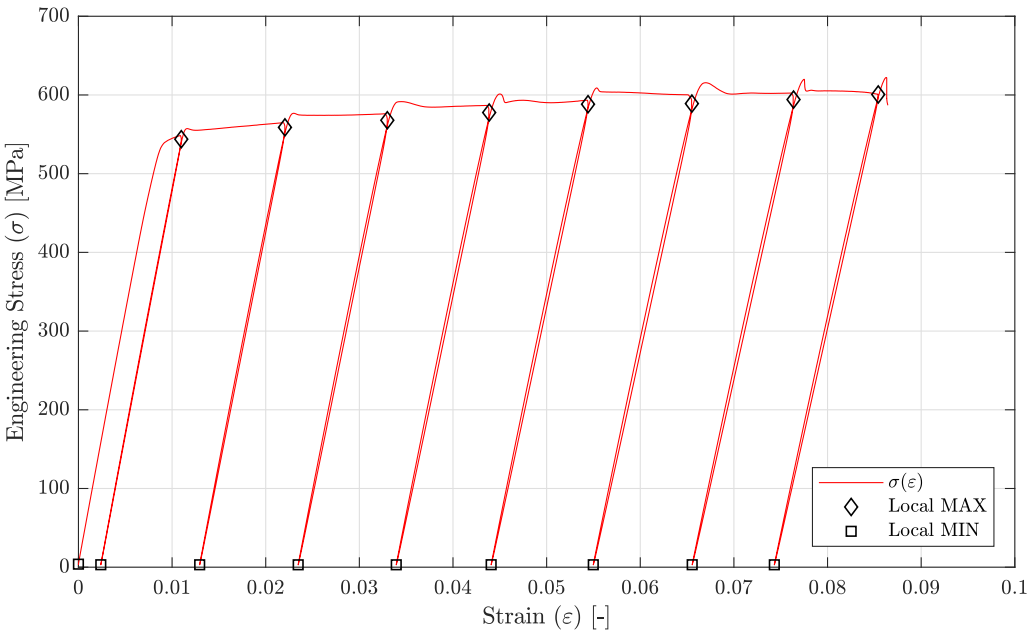

Figure 4.8: An interrupted tensile test with a 1% increment in strain after each cycle. The specimen shown is AA7075 from batch A age-hardened for 24 hours. A crosshead displacement of 1 mm/min was used. The squares and diamonds indicate the local minima and maxima between which the loading step occurred.

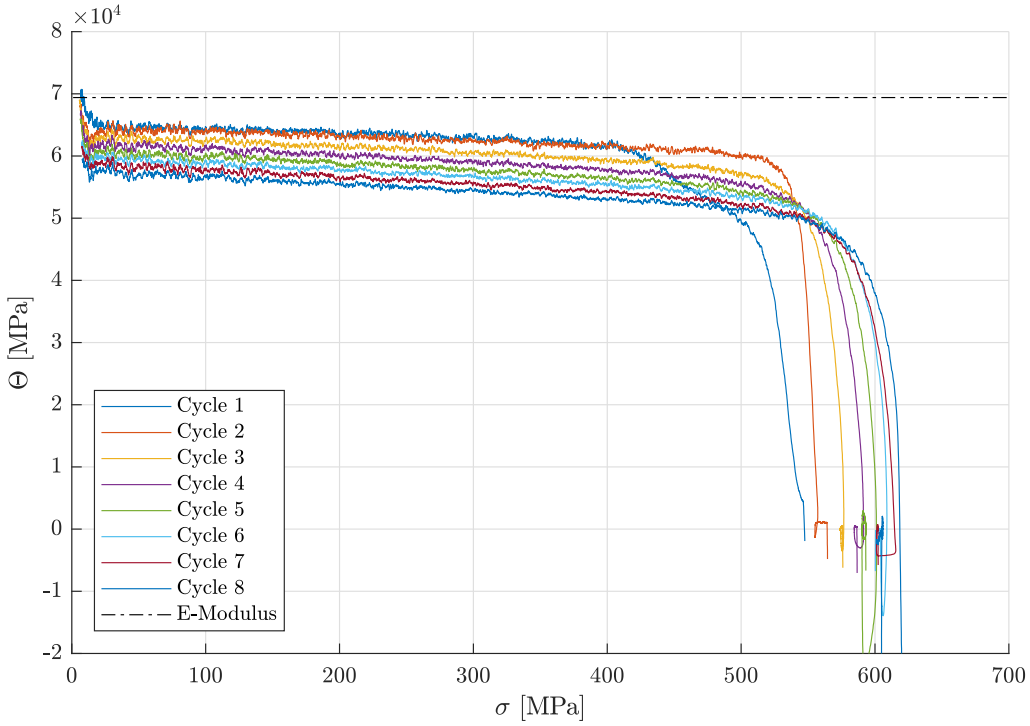

Figure 4.9: Extended Kocks-Mecking plots of the reloading steps of a cyclic tensile test. The curves shown were derived for the same specimen as in figure 4.8. The spiralling of the post-yield regime is attributed to the bulges in the tensile loading steps. The dashed line represents the Young's modulus $E = 69.4$ GPa. The last reloading step, which was not completed because of failure of the specimen, is not shown.

Figure 4.10 and 4.11 show the dislocation density and average segment length as a function of the plastic strain at the end of each unloading step. Figure 4.10 shows the quenched specimens from batch A and B, while figure 4.11 shows the specimens from batch B age-hardened for 16, 24 and 32 hours. Both figures show an increase in dislocation density as the plastic strain is increased. The average segment length decreases as the plastic strain increases. This behaviour corresponds to expectations based on dislocation theory and the trend also agrees with previous experimental results of Arechabaleta et al. [9]. The effects of the heat treatment times are also visible in figure 4.11. The specimens heat treated for longer periods of time have an increased dislocation density but a shorter average segment length.

4.2.2 Fitting the Taylor equation

The physical yield stress and dislocation density obtained from the loading cycles of the expiremement can be used to fit the Taylor equation (2.23). By fitting the data with this equation, σ_0 the contribution of all the strengthening mechanisms other than the strengthening due to dislocations, can be found. Typical results of this fit are shown in figure 4.12 where σ_0 is shown for specimens from batch A and B age-hardened for 16 hours. Results for other age-hardening times can be found in table 4.4. In figure 4.13 the change of σ_0 and α with the age-hardening time is shown. Specimens that were not heat treated after the solid solution treatment have a lower σ_0. Heat treated specimens exhibit a larger σ_0 where the heat treatment time seems to have little effect on the magnitude of σ_0 considering the time-scale used in the current investigation. The factor α is highest in the specimens that were not age-hardened and decreases as the hardening time increases. It is mostly in the range of the values proposed in literature (0.15-0.4) [3].

Table 4.4: The yield stress without dislocation contribution (σ_0) and the factor α of AA7075 heat treated at 0, 16, 24 and 32 hours.

	0h(A)	0h(B)	16h(A)	16h(B)	24h(A)	24h(B)	32h(A)	32h(B)
σ_0 [MPa]	285±28	304±21	463±6	452±14	493±7	462±16	493±3	468±16
α [-]	0.19±0.03	0.17±0.02	0.14±0.02	0.14±0.02	0.11±0.01	0.13±0.02	0.12±0.004	0.13±0.02

4.2.3 Anelastic strain during unloading

The anelastic strain during the unloading of each cycle was determined graphically according to figure 2.9 and plotted as a function of the physical yield stress (indicated as flow stress σ_f in the model of Torkabadi et al [2]) of the same cycle. This was done for all reloading cycles of specimens with the same heat treatment, the initial loading cycles of both specimens were averaged to determine σ_y. The data was fitted with equation (2.27) to obtain the fitting parameters $K = 2.6 \pm 0.17 \times 10^{-4}$ and $\varepsilon^{ae}_{pre} = 7.5 \pm 0.6 \times 10^{-4}$ with a coefficient of determination $R^2 = 0.96$. Subsequently an attempt was made to obtain L from equation (2.28), using α obtained from table 4.4 and ρ_0 from the expression $\varepsilon^{ae}_{pre} = \overline{M}^{-1} L^{-1} \rho_0 b A$, with $A = \pi L^2/8$. For the segment length an unrealistic value of $L = 6.35 \times 10^9$ m was calculated and thus for the initial dislocation density $\rho_i = 3.23 \times 10^{-3}$ m^{-2} an unrealistic value was found as well. These results, as well as the constitutive model of Torkabadi et al. will be discussed in section 5.4.1.

Figure 4.15 shows the anelastic strain introduced in the material during loading and the recovered anelastic strain during unloading. The anelastic loading strain was determined using equation (2.35) whereas the unloading strain was determined graphically according to figure 2.9. The anelastic unloading strain is smoother because it was obtained directly from the interrupted tensile test results. The fraction of unrecoverable anelastic strain according to equation (2.32) is also presented.

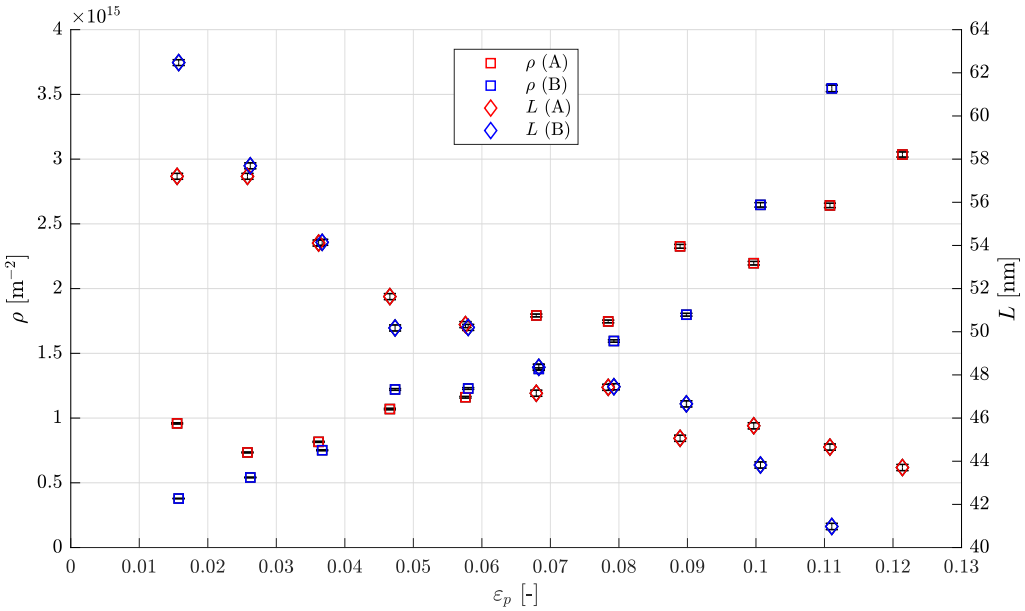

Figure 4.10: The dislocation density and average segment length as a function of the plastic strain of quenched AA7075 specimens from batch A and B. The data of the dislocation density were obtained from the fit of equation (2.20) to the extended Kocks-Mecking plot of each reloading curve. The average segment length was found from the critical stress and equation (2.21). Results from the initial loading curve are not included.

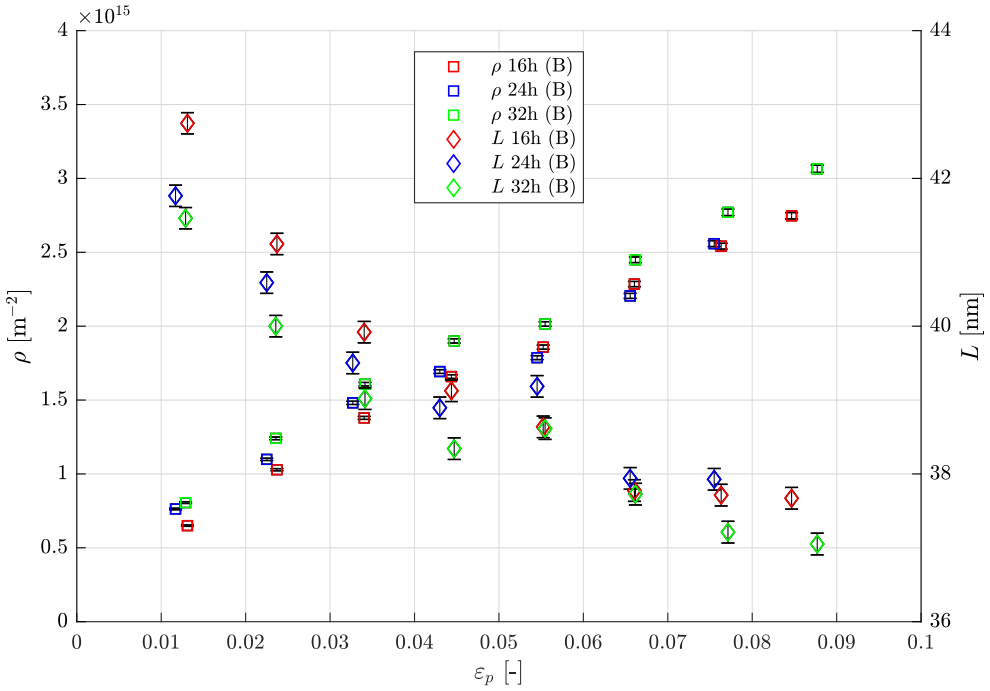

Figure 4.11: The dislocation density and average segment length as a function of the plastic strain of AA7075 specimens from batch A and B age-hardened for 16, 24 and 32 hours. The data of the dislocation density were obtained from the fit of equation (2.20) to the extended Kocks-Mecking plot of each reloading curve. The average segment length was found from the critical stress and equation (2.21). Results from the initial loading curve are not included.

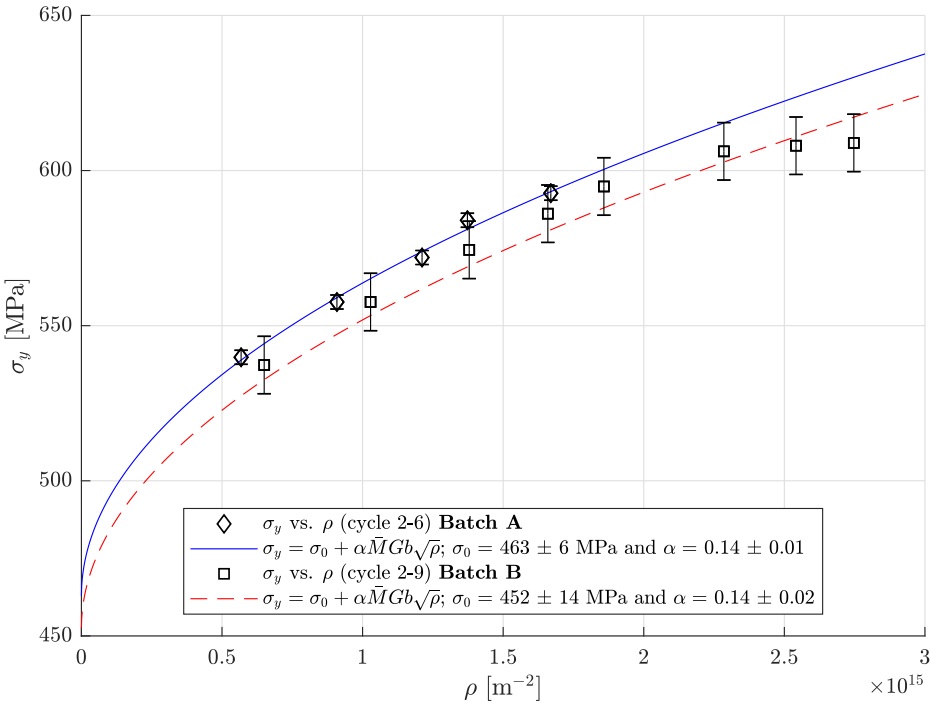

Figure 4.12: Fit of the Taylor equation (equation (2.23)) to the yield stresses of the reloading steps of the cyclic tensile test obtained using the abrupt change of slope. Results of two specimens are shown from batch A and B age-hardened for 16 hours. The initial loading curves are not included.

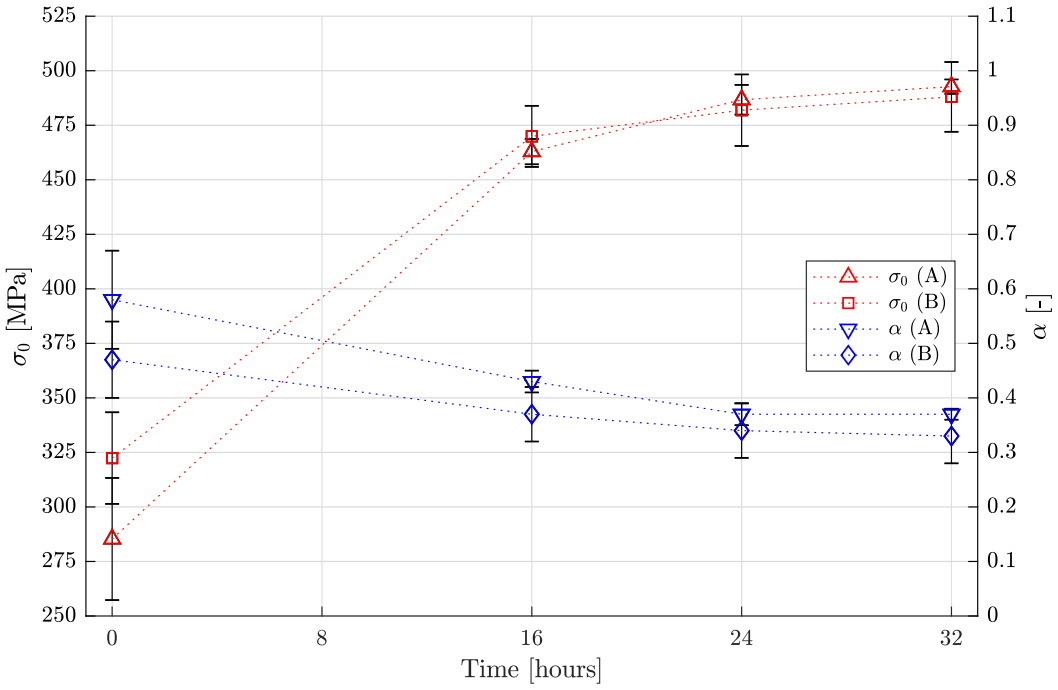

Figure 4.13: The strength contribution of all strengthening mechanisms except dislocation density (σ_0) and the factor α as function of the age-hardening time. The curves are shown for batch A and B.

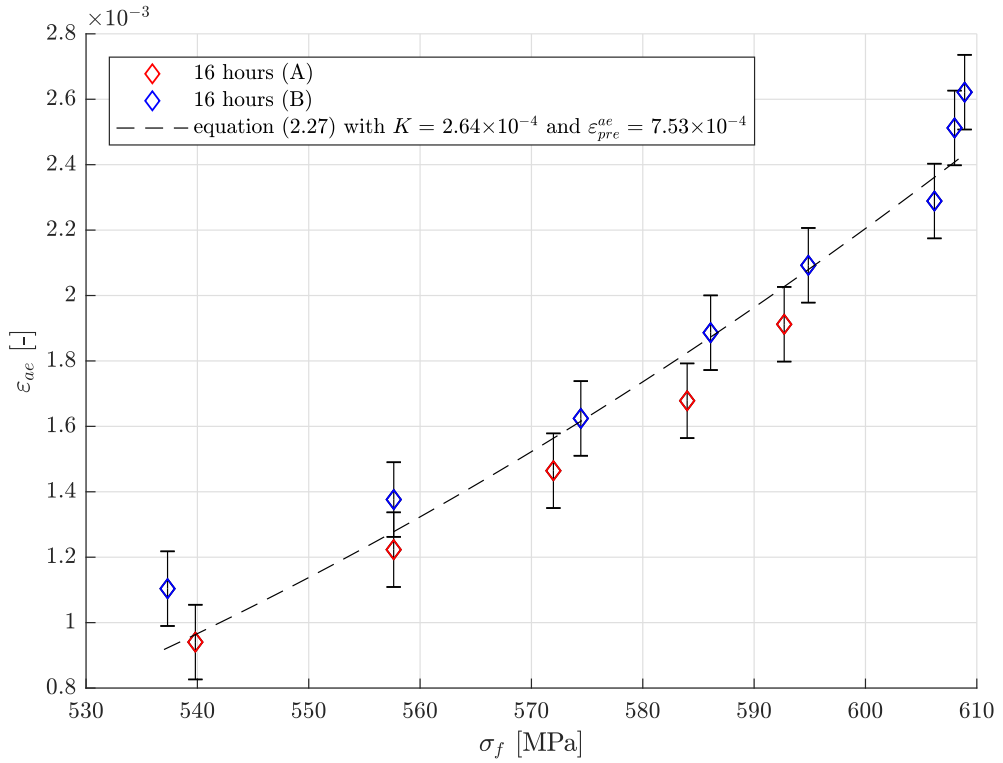

Figure 4.14: The anelastic strain as a function of the flow stress for a specimen aged at 16 hours, showing batch A and B. The dashed line is the fit of equation (2.27) according to the constitutive model of Torkabadi et al. [2]. The fitting parameters found for these specimens where: $K = 2.6 \pm 0.17 \times10^{-4}$ and $\varepsilon^{ae}_{pre} = 7.5 \pm 0.6 \times10^{-4}$, the coefficient of determination $R^2 = 0.96$.

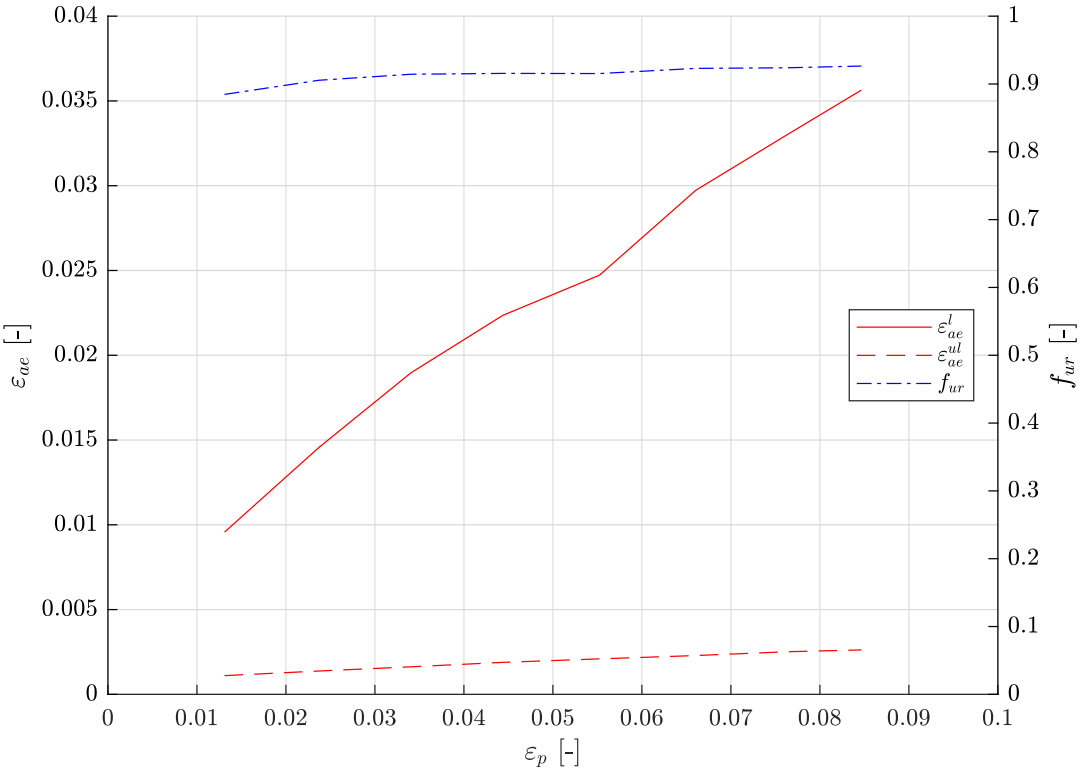

Figure 4.15: The anelastic strain during loading (ε_{ae}^{l}) and unloading (ε_{ae}^{l}) as function of the remaining plastic strain after unloading for a specimen aged at 16 hours from batch B. The fraction of unrecoverable anelastic strain (f_{ur}) is shown in blue.

CHAPTER 5

Discussion

The application of the physical yield criterion to the results of tensile tested aluminium and AA7075 is discussed first. After its applicability is confirmed the formation of bulges during interrupted tensile testing is discussed. Next the effects of precipitation hardened metal on the physical yield criterion are discussed. Subsequently, the recovery of anelastic strain during unloading and the constitutive model of Torkabadi et al. [2] are treated. Finally, the introduction of a segment length distribution is discussed and a number density is introduced.

5.1 The physical yield criterion for aluminium and AA7075

The physical yield criterion was successfully applied to the aluminium and AA7075 specimens with the exception of air-cooled aluminium. Note that, for the air cooled aluminium specimen a smaller strain rate could have resulted in a larger collection of data points which could in turn have resulted in a better defined pre-yield regime in the extended Kocks-Mecking plot. The quenched aluminium specimen and all the AA7075 specimens showed well defined Kocks-Mecking plots which could readily be fitted with the pre-yield anelastic modulus (equation (2.20)). This resulted in realistic values for ρ and L. The dislocation density is of the expected order of magnitude ($10^{14} - 10^{15}$ m^{-2}) and the dislocation segment length is of the same scale as the distance between precipitates found by Jacumasso et al. [43] and by Jung et al. [44]. Both investigated 7075-T6 alloys, which is equivalent to the 24 hour age-hardened specimens in the current investigation [35], using transmission electron microscopy (TEM). This means that the bowing out of dislocation lines between precipitates as pinning points rather than dislocation locks could have very well influenced the outcome of the physical yield criterion analysis.

5.1.1 Anomalies in tensile testing results

During tensile testing, one specimen artificially aged for 24 hours from batch A (24HA), showed a peculiar behaviour in the extended Kocks-Mecking plot. The plateau at low stress was found at a lower value for Θ and the physical yield stress was lower than other artificially age-hardened specimens. The main deviation in data was found in the strain rate, which was approximately half the rate of the other specimens. However the strain rate sensitivity of precipitated aluminium alloys is typically very low [45], meaning that the reduced strain rate of specimen 24HA is not likely the cause of the differences observed in the extended Kocks-Mecking plot. There was also no sign of slip in the grips of the tensile testing machine or any other visual evidence on the failed specimen. The deviation of the results of specimen 24HA in tensile testing was not further investigated.

5.2 Interrupted tensile testing experiments

The AA7075 specimens were cycled during an interrupted tensile test, with a 1% increase in plastic strain between each cycle. After the first reloading step bulges started to form at the

region where the transition from the pre-yield regime to the post-yield regime takes place. A phenomenon known as the unloading yield point effect [46–50]. This also influenced the shape of the extended Kocks-Mecking plot which was used to fit the pre-yield anelastic modulus to the loading data. The unloading yield point effect thus caused the spiralling of the extended Kocks-Mecking plot observed in figure 4.9. The spirals complicate the determination of the physical yield stress as the abrupt change of slope is no longer recognizable. To determine the physical yield stress an alternative approach was taken. The physical yield stress (σ_c) was introduced as a fitting parameter in equation (2.20). The minimum of the first spiral in the extended Kocks-Mecking plot was used as an initial guess for the physical yield stress in the least-squares fitting procedure and a fit was performed on the pre-yield regime of the extended Kocks-Mecking plot. Using this method the physical yield stress was determined with reasonable accuracy. However the use of an abrupt change of slope, if visible in the extended Kocks-Mecking plot, should always be preferred.

The unloading yield point effect has been extensively studied and is typically attributed to dislocation rearrangement during unloading or thermally activated migration of point defects to dislocations. Studies have been conducted on both single crystals [46–48] and polycrystals [49, 50]. The unloading yield point effect is more pronounced at lower temperatures [46]. In dislocation rearrangement, dislocations get locked during the unloading step. This can be for instance due to Lomer-Cottrell locks (section 2.1.2) [47] but also due to interaction with forest dislocations [48]. The effects of thermally activated migration of point defects considers a dislocation to which impurities or solute atoms diffuse. The solute atoms create extra pinning points along the dislocation line much like strain ageing. Nieh and Nix investigated the unloading yield point effect in an AA7075 alloy [50]. They reasoned that the unloading effects are not solely due to strain ageing effects and instead relate the effects of the unloading yield point effect to the the alloy content. A qualitative model was presented in [50] that describes the shearing of coherent precipitates in the matrix as a softening mechanism which is in competition with the strain hardening mechanisms. They propose that during unloading the shear precipitates heal and that as a result of this process the unloading yield point effect occurs [50].

The interupted tensile test results of Arechabaleta et al. [3] and Torkabadi et al. [2, 8, 32] also show the unloading yield point effect, albeit to a far lesser extent. Because the effects were less pronounced it is likely that the extended Kocks-Mecking plots they derived did show an abrupt change of slope that could be used to determine the physical yield stress. The main difference between the results of the current investigation and the investigations of Arechabaleta et al. and Torkabadi et al. is the strain rate during the interrupted tensile tests. However as discussed the strain rate sensitivity of precipitated aluminium alloys is low and the more pronounced yield point effect is more likely due to the mechanism described by Nieh and Nix [50]. Nevertheless investigating the effects of strain rate on the unloading yield point effect could also be of particular interest as simultaneously other strain rate effects could be studied. Additionally, further studies could be performed on the mechanism described by Nieh and Nix [50] and possible interactions between the mechanisms identified. The unloading yield point is most likely also related with dislocation behaviour during unloading and could as such be interesting in the investigation into anelastic unloading strain.

5.3 Effects of Precipitation hardening

The effects of precipitation hardening are clearly visible in figure 4.3, where the shift of the abrupt change of slope in the extended Kocks-Mecking plot can be observed. As expected, the specimens quenched after solution treatment without subsequent artificial age-hardening treatment show a lower physical yield stress in comparison to the age-hardened specimens. The difference between the artificial age-hardening times is however less pronounced. This is due to the fact that the overageing of AA7075 only occurs at times in excess of 50 hours, and only

really becomes pronounced at still longer times [51]. Hence a heat treatment with longer age-hardening times would have been more appropriate. Alternatively an increased temperature during artificial age-hardening could have been used to achieve an overaged state for some of the specimens.

5.3.1 Precipitates and the evolution of dislocation segment length

Precipitates are part of the dislocation pinning structure, their location hardly changes as a result of work hardening and as such the total dislocation pinning structure changes only partially as a result of plastic cycling during interrupted tensile tests. This partially fixed pinning structure was used to further investigate the work hardening behaviour of AA7075 due to dislocation interaction with the precipitate structure. Figures 4.10 and 4.11 show the evolution of the dislocation segment length with increased plastic strain for the quenched (0 hours) and artificially age-hardened specimens respectively. The quenched specimens have no precipitates in the microstructure, instead the alloying elements are in solid solutions. These solute atoms provide the main pinning points for dislocations [31]. The reduction of the segment length with plastic strain is however more pronounced for the quenched specimen ($\diamond$ in figure 4.10). This indicates that the dislocation structure is likely more predominant in the evolution of L with plastic strain. The artificially age-hardened specimens ($\diamond$ in figure 4.11) still show a reduction in segment length with increased plastic strain. Albeit this reduction is far less pronounced. This means that the evolution of the dislocation segment length is most likely predominantly governed by the distance that separates the precipitates. A distance that hardly changes with increased work hardening of the metal. Again the scale of the evolution of the dislocation segment length corresponds with observations in AA7075 alloys that have been age-hardened in similar ways [43, 44].

The Taylor equation can also be expressed as $\sigma_c = \sigma_0 + \alpha \overline{M} G b \sqrt{\rho}$. Arechabaleta et al. [3] reasoned that by excluding σ_0 the contribution of dislocations to the yield stress σ_d is:

$$\sigma_d = \frac{\overline{M} G b}{L_d} = \alpha \overline{M} G b \sqrt{\rho} \tag{5.1}$$

and thus:

$$\alpha = \frac{1}{L_d \sqrt{\rho}}. \tag{5.2}$$

L_d is the average distance between dislocations nodes when only dislocation self-interaction is considered. The dislocation density ρ and average L_d are thus closely related through α, which represents the dislocation structure quantitatively. Arechabaleta et al. also reasoned that, through the validation of the Taylor equation, α should remain constant even when the network changes. The decrease of L_d during work hardening is thus governed by α. The relation between L and L_d could be influenced by the precipitated microstructure and was therefore further investigated.

A specimen from batch B age-hardened for 16 hours (16B) was chosen for further investigation. The results of which are presented in figure 5.1. The values for α were calculated using the average dislocation segment length L obtained from the fit of the pre-yield anelastic modulus to the extended Kocks-Mecking plot and were not constant. Figure 5.1 shows the decrease of α with increased dislocation density calculated by equation (5.2) using the average dislocation segment length and dislocation density corresponding to the respective data point. The average dislocation segment length L calculated from the critical stress found from the extended Kocks-Mecking plot is thus not equivalent to L_d as α is not constant. Figure 5.2 shows the average dislocation segment length L (equation (2.21)) plotted against the dislocation density ρ. The respective values of the 16B specimen are shown as diamonds ($\diamond$) and equation (5.2) is plotted for three values of alpha (0.5; 0.75 and 0.9) and the substitution $L_d = L$. The decrease

of L with increasing dislocation density is too small to ensure a constant α. Here the partially changing dislocation pinning structure presumably plays a role. Because the precipitates in the metal form pinning points which do not move when the metal is work hardened, the evolution of the dislocation structure is impeded as a whole. This means that L remains larger than is necessary to maintain a constant value of α. This is because the precipitates fix part of the dislocation structure regardless of the work hardening. Equation (5.2) is therefore not suitable for application in a precipitated metal and a modification is required.

The steel alloy used by Arechabaleta et al. [3] was not precipitated and therefore the influence of precipitates was not considered. In a precipitated aluminium alloy the contribution of precipitate strengthening is included in σ_0 and since precipitation hardening is also based on dislocation interaction, σ_0 has to be incorporated in the case of age-hardened AA7075 alloys. If all other strengthening mechanisms, such as for instance grain boundary effects and solution hardening, are neglected so that σ_0 represents the precipitation hardening contribution σ_p alone, the Taylor equation can be rewritten as

$$\sigma_c = \sigma_p + \alpha \overline{M} G b \sqrt{\rho}. \tag{5.3}$$

The physical yield stress, σ_c, is found from the abrupt change of slope in the extended Kocks-Mecking plot. Therefore σ_c can be represented as

$$\sigma_c = \frac{\overline{M} G b}{L}, \tag{5.4}$$

where L is the average dislocation segment length shown in figure 5.2. In a similar way the stress due to precipitation hardening, based on the Orowan stress (section 2.3) can be expressed as

$$\sigma_p = \frac{\overline{M} G b}{L_p}, \tag{5.5}$$

where L_p is the average distance between precipitates. Equations (5.4) and (5.5) substituted in equation (5.3) give

$$\frac{\overline{M} G b}{L} = \frac{\overline{M} G b}{L_p} + \alpha \overline{M} G b \sqrt{\rho}. \tag{5.6}$$

Expressing equation (5.6) for α gives

$$\alpha = \frac{1}{\sqrt{\rho}} \left(\frac{1}{L} - \frac{1}{L_p} \right). \tag{5.7}$$

In equation (5.7) L_p is a constant which represents the average distance between precipitates and ρ and L are the dislocation density and average dislocation segment length calculated from the fit of the pre-yield anelastic modulus to each cycle of the interrupted tensile test respectively.

From figure 5.1 the calculated value $\sigma_0 = 452$ MPa can be used to determine L_p by using equation (5.5). A length of $L_p = 50.5 \pm 1.6$ nm was found. The scale of L_p is in agreement with the observations of Jacumasso et al. [43] and Jung et al. [44]. Subsequently α can be calculated for each cycle of the interrupted tensile test. It should be constant for each of the data points. A value of $\alpha = 0.14 \pm 0.01$ was found for cycles 2-9, the first cycle was not incorporated in the analysis. This corresponds with the value for α found in the Taylor equation fit (figure 4.12), validating equation (5.7). Equation (5.7) can be solved for L:

$$L = \left(\frac{1}{L_p} + \alpha \sqrt{\rho} \right)^{-1}, \tag{5.8}$$

which is plotted in figure 5.3 alongside the data of specimen 16B. The modified expression for α in equation (5.7) provides a more detailed quantitative description of the mixed dislocation pinning structure in a precipitation hardened alloy. Using L, ρ and L_p. A distinction can be made between the fixed dislocation pinning structure due to precipitates through the parameter L_p and the total dislocation pinning structure through L.

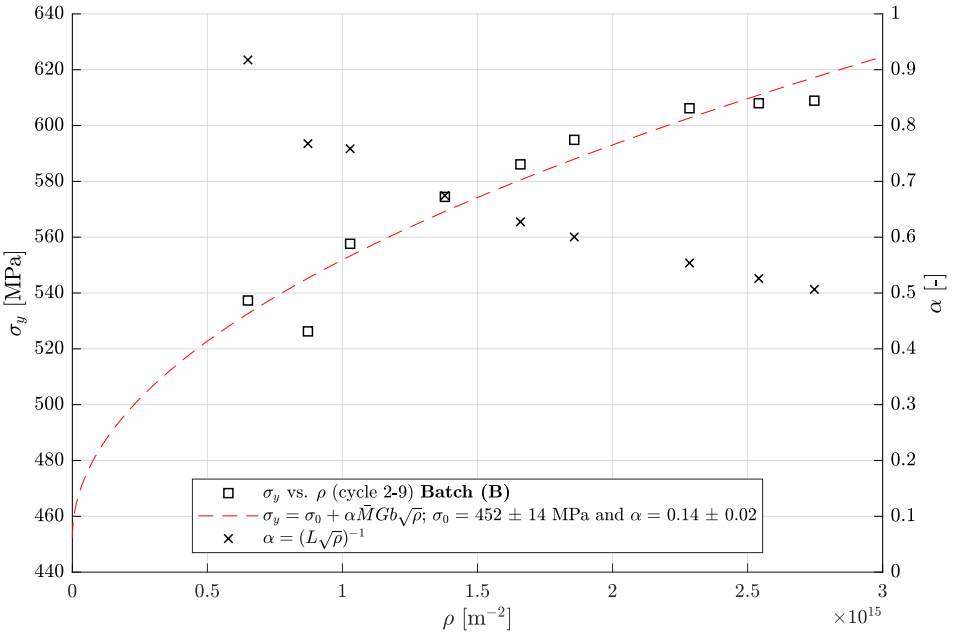

Figure 5.1: The physical yield stress of cycle 2-9 of a specimen hardened for 16 hours from batch B is shown for the respective dislocation density alongside the Taylor equation in red. α calculated with $L_d = L$ according to equation (5.2) is not constant.

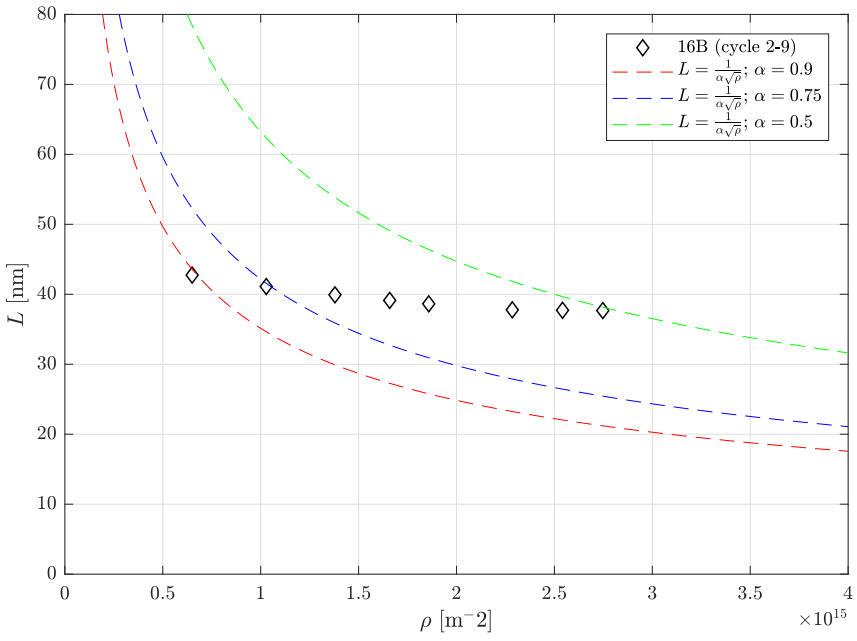

Figure 5.2: The relation between L and ρ for an age-hardened (16 hours, $\diamond$) specimen from batch B. Three curves are shown for constant values of α according to equation (5.2) with $L = L_d$. The calculated values for L ($\diamond$) do not follow the curves of constant α.

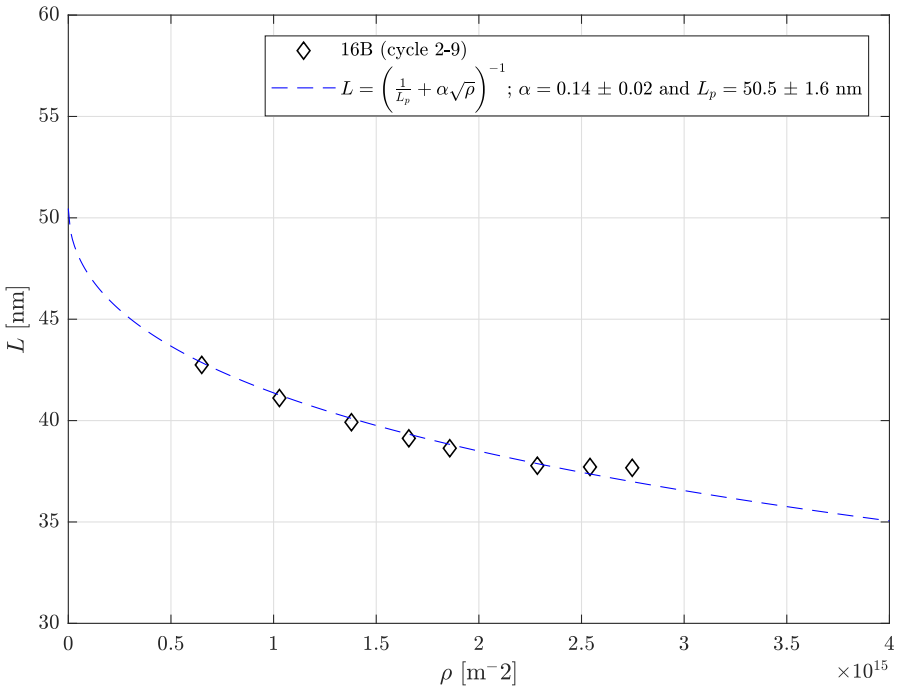

Figure 5.3: The relation between L and ρ for a specimen age-hardened for 16 hours (batch B) is shown alongside equation (5.8) with the values for α and L_p obtained through fitting of the Taylor equation and calculation using equation (5.5) respectively.

5.4 Anelastic Strain Recovery

During the loading and unloading steps of the specimen, the Frank-Read sources bow out and return to their equilibrium position respectively. When between loading and unloading plastic strain is introduced into the metal the average dislocation segment length reduces, as can be deduced from figure 4.10 and 4.11. In section 2.5 it was reasoned that during both loading and unloading the swept area of the dislocation at the critical state ($A = \pi L^2/8$) is related to the anelastic loading and unloading shear strain through equation (2.17). The introduction of the Taylor factor results in an expression for strain, rather than shear strain. The dislocation segment length decreases when plastic strain is introduced. Meaning that L at the onset of plastic deformation is larger than L at the initiation of unloading. By contrast the dislocation density increases as plastic strain is introduced.

From equation (2.35) the proportionality of the anelastic strain during loading is found to be the product of ρ and L. Under the assumption that the dislocation density and average dislocation segment length no longer change as soon as unloading is initiated. The dislocation density and segment length during the unloading step can be characterized by the fit of the pre-yield anelastic modulus to the extended Kocks-Mecking plot of the subsequent loading step. It could be expected that the anelastic unloading strain could also be expressed in terms of equation (2.17) using the dislocation density and segment length at the initiation of unloading. In that case the anelastic strain during the unloading of cycle one, should be equal to the anelastic loading strain of cycle two. From figure 4.15 it becomes apparent that this is not the case and that the anelastic unloading strain is smaller than the anelastic loading strain.

Equation (2.35) can be rewritten explicitly for A to arrive at an expression for the average swept area of a Frank-Read source prior to unloading such that the observed anelastic loading strain is accommodated

$$A_S^{UL} = \frac{\varepsilon_{UL}^{AE} L}{\rho b \overline{M}}, \tag{5.9}$$

where ρ and L are the dislocation density and average dislocation segment length obtained from the fit of the pre-yield anelastic modulus to the extended Kocks-Mecking plot of the subsequent loading step respectively. The average swept area represents the recoverable anelastic strain during unloading. Since the unloading strain is smaller than the loading strain in the subsequent loading step, the area is smaller than the area swept by a Frank-Read source of average dislocation segment of length L at its critical state during loading.

The next step is to consider that not all Frank-Read sources are exactly at their critical state at the moment unloading is initiated. This means that not all Frank-Read sources recover the maximal anelastic strain. This is one potential cause of the unrecoverable anelastic strain observed during interrupted tensile tests. Another consideration is that dislocation loops which have been emitted just before unloading still propagate through the metal as discussed in section 2.5.2. The propagation of these loops causes an anelastic strain in the loading direction and thus a negative anelastic unloading strain. This anelastic strain in opposing direction possibly undoes a portion of the anelastic unloading strain. A third option is that during the retraction of the dislocation segments of the Frank-Read sources during unloading, the returning dislocation segments can encounter a variety of pinning obstacles. When a retracting dislocation segment encounters such an obstacle it will spend some time waiting for thermal activation to occur before it can pass. The activation energy required is stress dependent and also the strain rate plays a role [52]. If the stress lowers at a sufficient rate the dislocation might remain stuck at the obstacle when the metal is fully unloaded because it can no longer obtain the energy required to pass. The Frank-Read source can then not fully return to its original position and not all anelastic strain is recovered. Rosenfield and Averbach [53] considered the specific case where the obstacle is a forest dislocation. When multiple dislocations try to glide back they can pile up at the forest dislocation. A back stress is exerted by the pile up on the tree. When a returning dislocation finally passes the forest dislocation it forms a jog. Hence Rosenfield and Averbach considered jog formation energy to quantify the anelastic unloading strain [53]. These three causes most likely happen simultaneously and together cause the unrecoverable anelastic strain during unloading.

5.4.1 Constitutive model of Torkabadi et al.

The constitutive model of Torkabadi et al. [2] was used to study the unloading behaviour of AA7075 in interrupted tensile testing. The anelastic strain retrieved after each cycle was determined graphically according to figure 2.9 and plotted against stress in figure 4.14. A fit to equation (2.27) was made, which resulted in values for K and ε_{pre}^{ae}. From these parameters, L and ρ_0 were determined according to:

$$L = \frac{K(\alpha G(2\overline{M})^{(3/2)})^2}{\pi b} \tag{5.10}$$

and

$$\rho_i = \frac{8\overline{M}\varepsilon_{pre}^{ae}}{b\pi L}. \tag{5.11}$$

The parameter K contains the average dislocation segment length L. However K is based on a fit to multiple data points (figure 4.14) all of which have a different value of L. Therefore L cannot be the dislocation segment length at the point of unloading. Because it is represented by a single value calculated using equation (5.10). Torkabadi et al. showed that the stress-strain curves of tensile and interrupted tensile tests overlap and as such the physical yield stress of each

loading step follows the post-yield regime in a tensile experiment [2]. This means that the yield stress of a reloading step is related to the flow stress at which the previous unloading step was initiated. The average dislocation length L at a flow stress σ_f thus can be calculated according to equation (2.21). So the average dislocation segment length changes as a function of the flow stress. Therefore L cannot be a constant but should in fact change with σ_f. This makes the constitutive model unsuitable for the physical modelling of the unloading of metals.

The values obtained for L and ρ_i calculated using equations (5.10) and (5.11) result in unrealistic values. For the dislocation segment length, $L = 6.35 \times 10^9$ m was found and for the initial dislocation density, $\rho_i = 3.23 \times 10^{-3}$ m^{-2}. This might be related to the fact that L is treated as a constant, which as discussed previously, it is not. The value found for α from figure 4.12, was used in equation (5.10) to find L. Since the expression in equation (5.11) also contains L the value found for ρ_i is also unrealistic. Despite the parameters K and ε^{ae}_{pre} not being suited for the calculation of the average dislocation segment length and the initial dislocation density for individual loading steps. The constitutive model of Torkabadi et al. is suited to determine the unloading modulus of a metal for springback simulation succesfully [2].

In the constitutive model of Torkabadi et al. [2] σ_0 is considered an unknown value which is eliminated by introduction of σ_y and ρ_i. However Arechabaleta et al. [3] found a way to obtain σ_0 by performing similar interrupted tensile tests. Results from a similar analysis on AA7075 are presented in figure 4.12 and table 4.4. An unloading model based on the Taylor equation (equation (2.23)), where L is a function of the physical yield stress through equation (2.21) could be considered as a next step. In this model, σ_0 can be readily used and no mathematical detours are required. Such a model could be used to study the effects of dislocations in the unloading of metals. It should however also take into account that the anelastic unloading strain is smaller than the loading strain as mentioned at the beginning of this section.

5.5 Distribution of dislocation segment length

In section 2.6 a continuous uniform length distribution was introduced in the normalized pre-yield anelastic modulus. The distribution of dislocation segment lengths is however never continuous uniform nor will each length be represented by a similar dislocation density as in the current model. The introduction of even such a basic distribution does however show that the the value of Θ (or T in the normalized situation) in the theoretical distribution model is not equal to zero at σ_c (or $s = 1$). Similar behaviour of Θ is observed for the data in figures 4.3, 4.6 and 4.7, where the onset of plastic deformation occurs at values of $\Theta > 0$. This means that it is possible that the dislocation segment length distribution is responsible for the abrupt change of slope at values of $\Theta > 0$ and that the value of Θ at σ_c is an indication of the distribution of segment lengths in the dislocation network. This would also mean that in the case of pure aluminium (figure 4.1) a distribution is hardly present, as Θ in the post-yield regime of the Kocks-Mecking curve is very close or equal to zero. In the interrupted tensile tests the unloading yield point effect and the spiralling in the Kocks-Mecking plot that ensues from it, make the graphical determination of the value of Θ_c not that obvious. For this reason the evolution of the dislocation segment length distribution could not be studied in this case.

5.5.1 Alternative distribution types

Lin et al. [54] investigated the dislocation segment length distribution of aluminium during creep by performing etch pitting and transmission electron microscopy experiments according to the method of Oden et al. [55]. They found a statistical distribution of dislocation segments from experimental data. The normalized analytical distribution for the dislocation segment length

distribution was further developed by Shi and Northwood [56]:

$$\Phi(u) = \beta^2 \rho^{-2} \left[2\rho L_m^{-2} \frac{L^2}{L_m^2} e^{-\frac{L^2}{L_m^2}} \right], \tag{5.12}$$

where $L_m = \frac{L_A}{2}\sqrt{\pi}$, with L_A the average dislocation segment length and β a constant including a dislocation network geometry factor. For tight uniform dislocation networks $\beta \approx 1$ and for non-uniform dislocation networks $\beta < 1$ [56]. To make the expression in equation (5.12) a function of u ($u = L/L_A$), the following substitution should be made: $L/L_m = \frac{2}{\sqrt{\pi}}u$. The implementation of this normalized distribution model in the physical yield criterion could prove valuable in gaining better insight in the dislocation structure from the extended Kocks-Mecking curve. Also by using interrupted tensile testing, the evolution of the dislocation structure during plastic strain could be characterized. The use of a statistical distributions which has been validated by experimental data is a good starting point for a realistic distribution of dislocation segment lengths in the pre-yield anelastic modulus.

The experimental distribution found by Lin et al. [54] shows resemblance with several other distribution types such as the log-normal, gamma or Weibull distribution. Naturally other length distributions similar to the experimental data can be used. Another adaptation that could be made to the current distribution is the use of a number density N, rather than the dislocation density ρ.

5.5.2 Number density length distribution

The introduction of a number density length distribution in the model of van Liempt and Sietsma [1] is similar to the steps described in section 2.6. Again a continuous uniform distribution is considered. However for the number density the box of the distribution is not fixed at the right side. Instead the average of u, u_0 is considered the center of the box of width $2w$ as depicted in figure 5.4. It was discussed previously that the continuous uniform distribution is a poor representation of the dislocation length distribution, however since the procedure is known it will be used as an example. To introduce the number density into the model, $\rho = NL$ has to be substituted in equation (2.37) such that the non-distributed normalized pre-yield anelastic modulus becomes:

$$T_{ND} = \frac{1 + \frac{V}{3}NL^3}{1 + VNL^3 S(s)}. \tag{5.13}$$

The expressions for V and $S(s)$ remain unchanged. The expression for u is instead normalized for the average length L_A ($u = L/L_A$) and $s = \sigma/\sigma_{cA}$ with σ_{cA} the stress corresponding to L_A. The normalized number density length distribution then can be expressed as:

$$T_D = \frac{1 + \frac{VL_A^3}{3}\int_0^1 N(u)u^3 \mathrm{d}u}{1 + VL_A^3 \int_0^1 N(u)u^3 \frac{su - \sqrt{1-(su)^2}\arcsin(su)}{(su)^3\sqrt{1-(su)^2}} \mathrm{d}u}. \tag{5.14}$$

For the general box distribution the solution of the integral in the numerator is $I(w,0) = \frac{1}{2w}\int_0^1 N(u)u^3 \mathrm{d}u = u_0(u_0^2 + w^2)$. The integral in the denominator also has an analytical solution, alike the distribution model in section 2.6, it is simpler and given by

$$I(w,s) = \frac{1}{2w}\int_0^1 N(u)u^3 \frac{su - \sqrt{1-(su)^2}\arcsin(su)}{(su)^3\sqrt{1-(su)^2}} \mathrm{d}u = \left[\frac{-2\sqrt{1-(su^2)} - su\arcsin(su)}{2ws^4} \right]_{u_0-w}^{u_0+w}. \tag{5.15}$$

The integral is normalized for the area of the box distribution $2w$ and introduced into equation (5.14). The solution of the integral in the numerator is also introduced, the expression for the normalized distributed pre-yield anelastic modulus is:

$$T_d = \frac{1 + \frac{V}{3} N_0 L_A^3 I(w, 0)}{1 + V N_0 L_A^3 I(w, s)}. \tag{5.16}$$

The number density provides a more intuitive way to express the distribution of segment lengths. The distribution $N(L)$ gives the number of dislocation of length L. A similar derivation can be performed for other type of distributions.

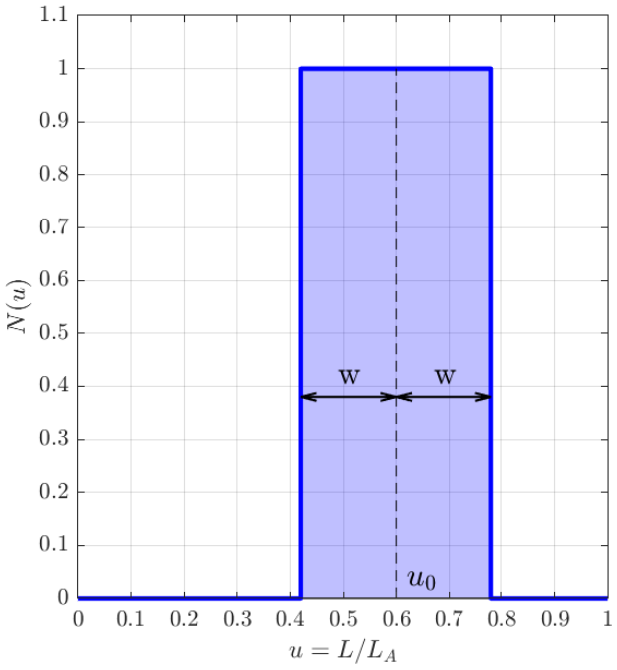

Figure 5.4: The continuous uniform number density distribution with the distribution parameters, u_0 and w.

CHAPTER 6

Conclusions and Recommendations

The effects of precipitates in the microstructure on dislocation behaviour and the development of the dislocation structure during work hardening of metals was investigated using tensile and interrupted tensile tests. The recovered anelastic strain after loading and unloading was investigated, as well as a distribution of dislocation segment lengths. An AA7075 aluminium alloy was chosen for the investigation, the alloy was artificially age-hardened for 0, 16, 24 and 32 hours to form different precipitate structures in the metal. Tensile tests were also performed on pure aluminium specimens. Models of van Liempt and Sietsma [1] and Torkabadi et al. [2] were used to study the dislocation behaviour during loading and unloading in interrupted tensile tests. Models were derived to study the recovery of anelastic strain and the distribution of dislocations using an adapted version of the pre-yield anelastic modulus. This chapter presents the conclusions drawn from the discussion on the results and recommendations for future research into this topic.

6.1 Conclusions

The conclusions drawn from the discussion of the present investigation into the effects of a precipitated microstructure on the application of the physical yield criterion, the development of the microstructure during work hardening and the recoverable anelastic strain are presented. The introduction of a dislocation length distribution in the physical yield criterion was also investigated. The conclusions can be summarized as follows.

(i) The physical yield criterion is suited to quantify the anelastic behaviour, physical yield stress, dislocation density and segment length of aluminium. Both pure aluminium and artificially age-hardened alloys were characterized successfully. The average dislocation segment length found from the fit of the pre-yield anelastic modulus to the Kocks-Mecking data was of a similar scale as observations with transmission electron microscopy. For very soft aluminium, the pre-yield regime might not be sufficiently recorded during a tensile test at high strain rates. This makes the application of the physical yield criterion difficult.

(ii) Precipitates provide a fixed dislocation pinning structure which does not change as work hardening is introduced. The evolution of the dislocation structure is impeded by this fixed structure which causes L to decrease at a lower rate whereby $\alpha = (L\sqrt{\rho})^{-1}$ is not constant, and $L \neq L_d$. The expression for α was modified to incorporate the impediment of the fixed pinning structure by taking $\alpha = \frac{1}{\sqrt{\rho}}(\frac{1}{L} - \frac{1}{L_p})$, with L_p the distance between fixed pinning points, in this case precipitates. The length L_p is related to σ_0 obtained from the Taylor equation. When the adapted expression for α was applied to the dislocation segment lengths obtained from the interrupted tensile tests, a constant value of $\alpha = 0.14$ was found, which is in agreement with the results from the Taylor equation fit. A precipitate distance of 50 nm was found, the scale of which corresponds with transmission electron microscopy observations of precipitates. Other strengthening effects such as grain boundary strengthening and solid solution strengthening were not considered.

(iii) The constitutive model of Torkabadi et al. [2] is not suited to study the physical behaviour of dislocations during unloading or the effects of dislocations on the anelastic unloading strain. The parameters K and ε_{pre}^{ae} were used to calculate the dislocation segment length L and initial dislocation density ρ_i, but this resulted in unrealistic values for both. K only returns a single value for L, which in reality changes with the flow stress. Therefore study on the change of L during plastic deformation is not possible using this model.

(iv) The introduction of a dislocation segment length distribution in the physical yield criterion model was proposed. The distribution model successfully showed that a distribution in the dislocation segment length causes $\Theta > 0$ at σ_c. The value of Θ at σ_c could therefore be an indication of the width of the dislocation segment length distribution.

6.2 Recommendations

Based on the results and conclusions of the current investigation, recommendations for further studies on the application of the physical yield criterion, the development of the microstructure during work hardening and the recoverable anelastic strain into the effects of a precipitated microstructure are presented. The recommendations also include those for the dislocation length distribution.

(i) The recovery of anelastic strain during unloading can currently not be studied because of the absence of a suitable unloading model. A physical model has to be developed to quantitatively analyse the behaviour of the anelastic strain during unloading. Such a model should take into account the possible causes that result in the observed unrecoverable anelastic strain during unloading in comparison to the anelastic loading strain. Namely, not all Frank-Read sources being at the critical state at initiation of unloading, the propagation of loops which causes portions of the anelastic loading strain to be neutralized and the fact that retracting dislocations could remain stuck behind obstacles in the microstructure.

(ii) The strain rate used in the interrupted tensile tests performed in the current investigation was different from earlier interrupted tensile tests in [2] and [3]. Despite the strain rate sensitivity of AA7075 being low, it might still have effects on the behaviour of dislocations during unloading. Dislocation segments getting stuck whilst returning to the equilibrium position of the Frank-Read source require thermal activation to pass the obstacles they encounter. The strain rate affects the thermal activation and thus the dislocation behaviour during unloading. Therefore, further investigation of the strain rate effects is recommended. Dislocation behaviour during unloading might in turn also influence the rearrangement of dislocations in the unloading yield point phenomenon.

(iii) When investigating a metal using the physical yield criterion and interrupted tensile tests it is advised to carefully consider unloading yield point effects in the metal. It might be necessary to take precautions to prevent the formation of pronounced bulges near the transition from pre-yield to post-yield regime which might disturb the fit of the pre-yield anelastic modulus to the pre-yield regime of the extended Kocks-Mecking plot.

(iv) Further development of the distribution model could help gain a better understanding of the shape of the dislocation network. A realistic expression for the distribution has to be incorporated in the model. The distribution should preferably be based on experimental data or expressions based on physical phenomena. Applying the distributed models on the Kocks-Mecking plots derived from interrupted tensile test could help to understand the evolution of the dislocation structure during plastic deformation better. The use of the number density should be preferred over the dislocation density during further development of the dislocation segment length distribution model.

References

[1] P. van Liempt and J. Sietsma, "A physically based yield criterion I. Determination of the yield stress based on analysis of pre-yield dislocation behaviour," *Materials Science and Engineering: A*, vol. 662, pp. 80–87, 2016.

[2] A. Torkabadi, P. van Liempt, V. T. Meinders, and A. H. van den Boogaard, *A constitutive model for the anelastic behavior of advanced high strength steels*, pp. 378–385. CIMNE, 2015.

[3] Z. Arechabaleta, P. van Liempt, and J. Sietsma, "Unravelling dislocation networks in metals," *Materials Science and Engineering: A*, vol. 710, pp. 329–333, 2018.

[4] C. M. Zener, *Elasticity and Anelasticity of Metals*. University of Chicago Press, 1948.

[5] A. K. Ghosh, "A physically-based constitutive model for metal deformation," *Acta Metallurgica*, vol. 28, no. 11, pp. 1443–1465, 1980.

[6] R. H. Wagoner, H. Lim, and M.-G. Lee, "Advanced issues in springback," *International Journal of Plasticity*, vol. 45, pp. 3–20, 2013.

[7] J. F. Wang, R. H. Wagoner, W. D. Carden, D. K. Matlock, and F. Barlat, "Creep and anelasticity in the springback of aluminum," *International Journal of Plasticity*, vol. 20, no. 12, pp. 2209–2232, 2004.

[8] A. Torkabadi, E. S. Perdahcıoğlu, and A. H. van den Boogaard, "Modelling of anelastic deformation in dual-phase steel for improved springback simulation," *Procedia Engineering*, vol. 207, pp. 185–190, 2017.

[9] Z. Arechabaleta, P. van Liempt, and J. Sietsma, "Quantification of dislocation structures from anelastic deformation behaviour," *Acta Materialia*, vol. 115, pp. 314–323, 2016.

[10] F. C. Frank, "Sessile dislocations," *Proceedings of the Physical Society. Section A*, vol. 62, no. 3, pp. 202–203, 1949.

[11] W. M. Lomer, "A dislocation reaction in the face-centred cubic lattice," *The London, Edinburgh, and Dublin Philosophical Magazine and Journal of Science*, vol. 42, no. 334, pp. 1327–1331, 1951.

[12] A. H. Cottrell, "LX. The formation of immobile dislocations during slip," *The London, Edinburgh, and Dublin Philosophical Magazine and Journal of Science*, vol. 43, no. 341, pp. 645–647, 1952.

[13] J. P. Hirth, "On dislocation interactions in the fcc lattice," *Journal of Applied Physics*, vol. 32, no. 4, pp. 700–706, 1961.

[14] E. Orowan, *Symposium on Internal Stresses in Metals and Alloys*, pp. 451–453. The Institute of Metals, 1948.

[15] D. Hull and D. J. Bacon, *Introduction to Dislocations*. Elsevier, 2011.

[16] F. C. Frank *Physica*, vol. 62, no. 3, pp. 202–203, 1949.

[17] N. Thompson, "Dislocation nodes in face-centred cubic lattices," *Proceedings of the Physical Society. Section B*, vol. 66, no. 6, pp. 481–492, 1953.

[18] J. P. Hirth and J. Lothe, *Theory of dislocations*. John Wiley & Sons, New York, 2nd ed., 1982.

[19] G. Gottstein, *Physical Foundations of Materials Science*. Springer, Berlin, 2004.

[20] P. van Liempt, C. Bos, and J. Sietsma, "A physically based yield criterion II. Incorporation of Hall Petch effect and resistance due to thermally activated dislocation glide," *Materials Science and Engineering: A*, vol. 652, pp. 7–13, 2016.

[21] J. Friedel, *Dislocations*. Pergamon Press, 1964.

[22] F. C. Frank and W. T. Read, "Multiplication processes for slow moving dislocations," *Physical Review*, vol. 79, no. 4, pp. 722–723, 1950.

[23] M. F. Ashby, "Results and consequences of a recalculation of the Frank-Read and the Orowan stress," *Acta Metallurgica*, vol. 14, no. 5, pp. 679–681, 1966.

[24] G. Schoeck, "Dislocation theory of plasticity of metals," in *Advances in Applied Mechanics*, pp. 229–279, Elsevier, 1956.

[25] A. H. Cottrell, *Deformation of solids at high rates of strain*, pp. 1–12. The Institution of Mechanical Engineers, 1957.

[26] F. Kroupa, "Dislocation dipoles and dislocation loops," *Le Journal de Physique Colloques*, vol. 27, pp. 154–167, jul 1966.

[27] C. Goulas, C. Jiménez-Peña, F. Castro-Cerda, M. G. Mecozzi, D. Debruyne, R. Petrov, and J. Sietsma, "The effect of shot peening on 51CrV4 with bainitic and tempered martensitic microstructure," *Journal of Materials Processing Technology*, Submitted for publication.

[28] B. L. Ennis, E. Jimenez-Melero, E. H. Atzema, M. Krugla, M. A. Azeem, D. Rowley, D. Daisenberger, D. N. Hanlon, and P. D. Lee, "Metastable austenite driven work-hardening behaviour in a TRIP-assisted dual phase steel," *International Journal of Plasticity*, vol. 88, pp. 126–139, 2017.

[29] B. L. Ennis, C. Bos, M. P. Aarnts, P. D. Lee, and E. Jimenez-Melero, "Work hardening behaviour in banded dual phase steel structures with improved formability," *Materials Science and Engineering: A*, vol. 713, pp. 278–286, 2018.

[30] U. F. Kocks and H. Mecking, "Physics and phenomenology of strain hardening: the FCC case," *Progress in Materials Science*, vol. 48, no. 3, pp. 171–273, 2003.

[31] D. A. Porter, K. E. Easterling, and M. Sherif, *Phase Transformations in Metals and Alloys*. CRC Press, 3rd ed., 2009.

[32] A. Torkabadi, V. T. Meinders, and A. H. van den Boogaard, "On the nonlinear anelastic behaviour of AHSS," *Journal of Physics: Conference Series*, vol. 734, p. 032100, 2016.

[33] A. Ghaei, D. E. Green, and A. Aryanpour, "Springback simulation of advanced high strength steels considering nonlinear elastic unloading–reloading behavior," *Materials & Design*, vol. 88, pp. 461–470, 2015.

[34] U. Messerschmidt, *Dislocation Dynamics During Plastic Deformation*. Springer Berlin Heidelberg, 2010.

[35] J. R. Davis, ed., *ASM Specialty Handbook Aluminum and Aluminum Alloys*. ASM International, 1993.

[36] C. B. Scruby and B. C. Moss, "Non-contact ultrasonic measurements on steel at elevated temperatures," *NDT & E International*, vol. 26, no. 4, pp. 177–188, 1993.

[37] U. F. Kocks, "The relation between polycrystal deformation and single-crystal deformation," *Metallurgical and Materials Transactions B*, vol. 1, no. 5, pp. 1121–1143, 1970.

[38] C. Comte and J. von Stebut, "Microprobe-type measurement of Young's modulus and Poisson coefficient by means of depth sensing indentation and acoustic microscopy," *Surface and Coatings Technology*, vol. 154, no. 1, pp. 42 – 48, 2002.

[39] E. Kim and H. Changani, "Study of dynamic mechanical behavior of aluminum 7075-T6 with respect to diameters and l/d ratios using Split Hopkinson Pressure Bar (SHPB)," *Structural Engineering and Mechanics*, vol. 55, no. 4, pp. 857–869, 2015.

[40] H. J. Axon and W. Hume-Rothery, "The lattice spacings of solid solutions of different elements in aluminium," *Proceedings of the Royal Society A: Mathematical, Physical and Engineering Sciences*, vol. 193, no. 1032, pp. 1–24, 1948.

[41] J. L. Murray and A. J. McAlister, "The Al-Si (aluminum-silicon) system," *Bulletin of Alloy Phase Diagrams*, vol. 5, no. 1, pp. 74–78, 1984.

[42] L. F. Mondolfo, N. A. Gjostein, and D. W. Levinson, "Structural changes during the aging in an Al-Mg-Zn alloy," *Journal of Metals*, vol. 8, no. 10, pp. 1378–1385, 1956.

[43] S. C. Jacumasso, J. de Paula Martins, and A. L. M. de Carvalho, "Analysis of precipitate density of an aluminium alloy by TEM and AFM," *REM - International Engineering Journal*, vol. 69, no. 4, pp. 451–457, 2016.

[44] S.-H. Jung, J. Lee, and M. Kawasaki, "Effects of pre-strain on the aging behavior of al 7075 alloy for hot-stamping capability," *Metals*, vol. 8, no. 2, p. 137, 2018.

[45] L. D. Oosterkamp, A. Ivankovic, and G. Venizelos, "High strain rate properties of selected aluminium alloys," *Materials Science and Engineering: A*, vol. 278, no. 1-2, pp. 225–235, 2000.

[46] P. Haasen and A. Kelly, "A yield phenomenon in face-centered cubic single crystals," *Acta Metallurgica*, vol. 5, no. 4, pp. 192–199, 1957.

[47] M. J. Makin, "Unloading effects in the plastic properties of copper single crystals," *Philosophical Magazine*, vol. 3, no. 27, pp. 287–301, 1958.

[48] H. K. Birnbaum, "Unloading effects in crystals—I The unloading yield point effect," *Acta Metallurgica*, vol. 9, no. 4, pp. 320–326, 1961.

[49] A. T. Thomas, "Unloading effects in aluminium and aluminium-zinc single crystals," *Philosophical Magazine*, vol. 5, no. 57, pp. 947–966, 1960.

[50] T. G. Nieh and W. D. Nix, "Unloading yield effects in aluminum alloys," *Metallurgical Transactions A*, vol. 17, no. 1, pp. 121–126, 1986.

[51] M. M. Shea and B. V. N. Rao, "Enhanced age hardening of 7075 aluminum alloy after ultrasonic vibration," *Materials Science and Engineering*, vol. 61, no. 1, pp. 67–77, 1983.

[52] U. F. Kocks, "Plastic deformation: Thermal activation approach," in *Encyclopedia of Materials: Science and Technology*, pp. 7084–7088, Elsevier, 2001.

[53] A. R. Rosenfield and B. L. Averbach, "Non-elastic unloading of copper and aluminum," *Acta Metallurgica*, vol. 10, no. 1, pp. 71–74, 1962.

[54] P. Lin, S. S. Lee, and A. J. Ardell, "Scaling characteristics of dislocation link length distributions generated during the creep of crystals," *Acta Metallurgica*, vol. 37, no. 2, pp. 739–748, 1989.

[55] A. Oden, E. Lind, and R. Lagneborg, "Dislocation distributions during creep and recovery of a 20%Cr-35%Ni steel at 700°C," 1974.

[56] L. Shi and D. O. Northwood, "On dislocation link length statistics for plastic deformation of crystals," *Physica Status Solidi (a)*, vol. 137, no. 1, pp. 75–85, 1993.